The Late Paleozoic Ice Age in western equatorial Pangea: context for complex interactions among aeolian, alluvial, and shoreface sedimentary environments during the Late Pennsylvanian - early Permian

Marie Olivier, Sylvie Bourquin, Guy Desaubliaux, Celine Ducassou, Camille Rossignol, Gautier Daniau, Dan Chaney

Journal Pre-proofs

The Late Paleozoic Ice Age in western equatorial Pangea: context for complex interactions among aeolian, alluvial, and shoreface sedimentary environments during the Late Pennsylvanian - early Permian

Marie Olivier, Sylvie Bourquin, Guy Desaubliaux, Celine Ducassou, Camille Rossignol, Gautier Daniau, Dan Chaney

PII: S1342-937X(23)00192-2
DOI: https://doi.org/10.1016/j.gr.2023.07.004
Reference: GR 3091

To appear in: *Gondwana Research*

Received Date: 2 December 2022
Revised Date: 19 May 2023
Accepted Date: 7 July 2023

Please cite this article as: M. Olivier, S. Bourquin, G. Desaubliaux, C. Ducassou, C. Rossignol, G. Daniau, D. Chaney, The Late Paleozoic Ice Age in western equatorial Pangea: context for complex interactions among aeolian, alluvial, and shoreface sedimentary environments during the Late Pennsylvanian - early Permian, *Gondwana Research* (2023), doi: https://doi.org/10.1016/j.gr.2023.07.004

The Late Paleozoic Ice Age in western equatorial Pangea: context for complex interactions among aeolian, alluvial, and shoreface sedimentary environments during the Late Pennsylvanian - early Permian

Marie Olivier[(1)], Sylvie Bourquin[(1)*], Guy Desaubliaux[(2)], Celine Ducassou[(1)], Camille Rossignol[(3)], Gautier Daniau[(4)], Dan Chaney[(5)]

[(1)] Univ. Rennes, CNRS, Géosciences Rennes – UMR CNRS 6118, F-35000 Rennes, France

[(2)] CVA, Engineering, Tour Egée, 9/11 allée de l'arche, 92671 Courbevois cedex 105, France

[(3)] Università degli Studi di Cagliari, Dipartimento di Scienze Chimiche e Geologiche, Cittadella Universitaria, 09042 Monserrato (Ca), Italy

[(4)] ENGIE, 1 place Samuel de Champlain, 92930 Paris – La Défense, France

[(5)] NMNH – MRC-121, Department of Paleobiology, Smithsonian Institution, Washington, DC 20013-7012, USA; current address: 7525 Prairie Road NE, Albuquerque, NM 87109

[*] Corresponding author

Abstract

The evolution of depositional environments in the Late Pennsylvanian-early Permian of the Paradox Basin in Utah, USA, is investigated through detailed sedimentological and high-resolution sequence stratigraphic analyses, in order to define a model of landscape evolution, to discuss the stratigraphic model, and to evaluate the significance of the cyclicity in the paleoclimatic context. Forty high-resolution cycles integrated in 15 minor and two major cycles are observed for the first time throughout the Late Pennsylvanian-early Permian units. A-three steps landscape evolution is recognized. First, the lower Cutler beds, mainly corresponded to a marine environment, with longshore bar, subtidal, tidal, mouth-bar, and with locally fluvial deposits. The upper part of the lower Cutler beds also contains an aeolian dune. Second, the Cedar Mesa Sandstone, corresponded to broad erg deposits which are present across the entire study area, whereas longshore bar, subtidal, mouth-bar, and some fluvial deposits are mainly preserved in the northern part of the studied area. Third, the Organ Rock Formation records decreasing aeolian dune field preservation. To the south, the aeolian environments are interbedded with shoreface deposits, whereas to the north, fluvial deposits with some mouth-bars are more developed. Semi-arid climatic conditions persisted, as indicated by the presence of calcretes. Everywhere in these three steps, root traces within sandstone bars indicate that a soil was once present above the sand dunes. This new model of landscape evolution documents complex interactions between aeolian, fluvial and marine environments within the entire Permian succession of the Paradox Basin. High-resolution

stratigraphic analyses allow to discuss the significance of the cyclicity in a scenario that take into consideration sea-level variation in the Late Paleozoic Ice Age paleoclimatic context. This Late Pennsylvanian to early Permian succession reflects both relative sea-level fluctuations and the variability of sediment supply.

Keywords

High-resolution sequence stratigraphy; Sea-level variation; Palaeoenvironment; Palaeoclimate

1. Introduction

Since the early 1990's, the concept of high-resolution sequence stratigraphy, initially defined in marine environments (Jervey, 1988, Posamentier & Vail 1988, Posamentier *et al.* 1988, Van Wagoner *et al.* 1988), has been applied to continental environments (e.g. Shanley & McCabe, 1993, 1994; Wright & Marriott, 1993; Leeder & Stewart, 1996; Catuneanu *et al.*, 2009). Studies on the accumulation and preservation of aeolian deposits have focused mainly on the relationship between dry and wet climatic cycles, as reflected by water-table variations. The development of sequence stratigraphy in aeolian systems involves studying the relationship between water-level, subsidence and change in sediment availability (e.g. Yang & Nio, 1993; Kocurek & Havholm, 1993; Havholm et al., 1993; Blakey, 1996; Carr-Cabaugh & Kocurek, 1998; Veiga *et al.*, 2002). Several models propose either an interaction between aeolian, fluvial and lacustrine (e.g. Clemmensen *et al.*, 1989; Tirsgaard & Oxnevad, 1998; Sweet, 1999; Mountney & Jagger, 2004; Bourquin *et al.*, 2009; Hême de Lacotte & Mountney, 2022), or aeolian and marine environments (Blanchard *et al.*, 2016). Some models discuss the interaction between all three, aeolian, marine and fluvial deposits (e.g. Rankey 1997; Jordan & Mountney, 2010; 2012; Wakefield & Mountney, 2013 and the pioneering work of Terrell, 1972) and their relation through time and space. Other models at reservoir scale study the interaction between water table and sediment supply changes and dune-field events driven by autogenic mechanisms or allogenic forcing (e.g. Gross et al., 2022; Mountney, 2006).

The Pennsylvanian – Permian Paradox Basin, part of the Colorado Plateau located near the Four Corners area, between Utah, Colorado, New Mexico and Arizona (Fig. 1), is characterized by well-exposed outcrops. The Late Pennsylvanian - Permian succession (Fig. 2) has been the focus of many studies since the pioneering works of Wengerd & Matheny (1958), Orgill, (1971), Terrell, 1972), Baars (1962), Loope (1981), and Mack (1977). The lower part (lower Cutler beds) is classically considered to comprise shallow marine, aeolian, and fluvial deposits, and overlying deposits are considered to be exclusively continental (e.g. Soreghan *et al.*, 2002a; Jordan & Mountney, 2010; Wakefield & Mountney, 2013). The middle part is considered as dominated by aeolian deposits (Cedar Mesa Sandstone; e.g. Mountney & Jagger, 2004; Mountney, 2006; Jordan & Mountney, 2010), and the upper part by mainly fluvial deposits of the Organ Rock Formation, Fm (e.g. Moore *et al.*, 2008; Soreghan et al., 2009; Keiser et al., 2015; Venus *et al.*, 2015). Marine deposits reappear at the top of the succession (White Rim Sandstone; e.g. Steele, 1987; Chan, 1989). This Late Pennsylvanian - Permian succession was deposited during the Late Paleozoic Ice Age (LPIA; Fielding *et al.*, 2008; Montañez *et al.*, 2016; Griffis et al., 2022) and is located in the central Pangean equatorial region (Soreghan et al., 2020). In consequence, these early Permian series

provide an opportunity to study the variation of depositional environments, vegetation preservation and stratigraphic cycles considering sea-level, tectonics and sediment supply variations within glacial-interglacial phases in the equatorial Pangea.

Based on study of Late Pennsylvanian - early Permian strata of the Canyonlands National Park in Utah (Fig. 1), the aim of this paper is to reinterpret the palaeoenvironment evolution in space and time and to define a high-resolution sequence stratigraphy in an equatorial context during a glacial-interglacial period. From a detailed sedimentological study, the specific objectives are to: (1) describe the evolution of depositional environments, (2) define the high-resolution stratigraphic cycles and surfaces, (3) propose stratigraphic correlations and a model of landscape evolution of the Late Pennsylvanian to the early Permian succession, and (4) discuss a stratigraphic model and the significance of cyclicity in the LPIA paleoclimatic context.

2. Geological setting

The Pennsylvanian – Permian Paradox Basin was bounded by three main tectonic uplifts that occurred during the Early Pennsylvanian and formed the Uncompahgre Highland, and Defiance-Zuni Uplift and Emery Uplift (Wengerd & Matheny, 1958; Baars, 1962). These highlands (Fig. 1C) are onlapped by Permian strata, hence forming a major unconformity within the Colorado Plateau (Wengerd & Matheny, 1958). The Uncompahgre Highland constituted the highest relief during Pennsylvanian and Permian time and therefore the main source of sediments supplying the basin until the late Leonardian, i.e. late Cisuralian, – early Guadalupian (Wengerd & Matheny, 1958).

In the Paradox Basin (Figs. 1, 2), Permian deposits overlie the Hermosa Group (Gp) except in the northeast part of the basin, where they rest on the Proterozoic basement, and in the west where they unconformably overlie the Mississippian formations (Condon, 1997). Since Loope (1984) questioned the existence of the unconformity defined by Baars (1962), the Hermosa Gp is considered to be conformably overlain by a transitional unit between underlying predominantly marine deposits and the overlying continental deposits of the Cutler Gp. This transitional unit is named the lower Cutler beds, which represents an informal terminology now widely accepted (see discussion in Jordan & Montney, 2010). Lower Middle Triassic (Moenkopi Fm), or Upper Triassic (Chinle Fm) strata unconformably overlie the Permian (Fig. 2; Condon, 1997).

In the Colorado Plateau, the Permian deposits are characterised by marine and terrestrial sediments grading into each other laterally and vertically (Condon, 1997). The important work of Baker & Reeside (1929) proposed regional stratigraphic correlations within the Colorado Plateau that are still in use today. For the present study, the nomenclature of Baars (1962) is used for the Canyonland section (Fig. 2), integrating the modifications of Loope (1984).

In the Canyonlands National Park (Fig. 1) the Cutler Gp (Fig. 2) is divided into five formations (Wengerd & Matheny, 1958; Baars, 1962; Baars & Molenaar, 1971). The lower Cutler beds, previously named Rico Fm, Wolfcampian Carbonates, or Elephant Canyon Fm, are considered to be of Late Pennsylvanian to early Cisuralian (i.e. Missourian to lower Wolfcampian, e.g. Soreghan *et al.*, 2002a, DiMichele *et al.*, 2014). This formation is preserved from southeastern Utah to the San Rafael Swell to the northwest (Loope, 1984;

Sanderson & Verville, 1990). The Cedar Mesa Sandstone (Fig. 2) is composed almost entirely of sandstones. The Organ Rock Fm (Fig. 2) is laterally equivalent to the Hermit Shale of the Grand Canyon, attributed to late Wolfcampian to early Leonardian, i.e. Cisuralian, on the basis of vertebrate fragments (Vaughn, 1964), plant remains (White, 1929), and conodonts (Lucas & Henderson, 2021). The White Rim Sandstone overlies the Organ Rock Fm and thins to a further-edge directly below dead Horse point, and is present further northeast in the subsurface (Baars, 1987). The Undivided Cutler Gp south and west of the Uncompahgre Highland, north-eastward of Moab (Figs. 1, 2), was considered to be deposited from the Upper Pennsylvanian to the Cisuralian (e.g. Moore *et al.*, 2008). To the northeast of Moab, the Organ Rock Fm disappears and the Cedar Mesa Sandstone is directly overlain by White Rim Sandstone (e.g. Baars & Molenaar, 1971; Loope, 1984).

The lower Cutler beds consist of mixed shallow marine fossiliferous limestones and continental red beds that comprise aeolian and fluvial sediments (Jordan & Mountney, 2010). A varied marine faunal assemblage, including brachiopods, bivalves, crinoids and bryozoans, indicates open marine conditions (Terrell, 1972). For Wakefield & Mountney (2013), laterally extensive and continuous shallow-marine packages that can be correlated over > 5000 km^2 represent the maximum of transgression during the deposition of the lower Cutler beds over a coastal plain of very low relief and seaward dip. In the southern Paradox Basin, Soreghan *et al.* (2002a) interpret this formation as composed predominantly of loessite locally reworked by fluvial and marine processes. The top of lower Cutler beds is defined as a prominent, laterally extensive, marine limestone, named Shafer Limestone, deposited during the last major northeastward marine transgression into the basin, above which lie exclusively non-marine sediments of the Cedar Mesa Sandstone (Mountney & Jagger, 2004; Mountney, 2006; Jordan & Mountney, 2010).

The Cedar Mesa Sandstone is in part composed of large cross-bedded sandstone bodies. The depositional environment for these sandstones is debated. Early authors (Gregory, 1938; Kunkel, 1958; Wengerd & Matheny, 1958; Baars, 1962; Baars & Molenaar, 1971; Mack, 1977, 1979) suggested that they were either aeolian dunes or marine longshore bar deposits based on the presence of large–scale cross beds, convolute bedding, foraminifers, rare crinoid ossicles, or occasional glauconite grains. Baars (1962, 1979) and Mack (1977, 1978, 1979) proposed that the Cedar Mesa Sandstone is, at least in part, shallow littoral marine. However, Loope (1981, 1984) interpreted all the sand dunes of the Rico Fm, i.e. lower Cutler beds and Cedar Mesa Sandstone, composed of well-sorted fine-grained quartz arenite characterized by thick cross-stratified beds as aeolian dunes. He argued convincingly for a predominantly non-marine aeolian erg and erg margin origin for the Cedar Mesa Sandstone, noting the occurrence of rhizolith horizons as strong evidence for a terrestrial depositional setting, with prevailing paleowinds from (present day coordinates) northwest to southeast. However, Baars (1987) suggested that Cedar Mesa Sandstone is coastal deposit, corresponding to a complex environment in which near-shore marine conditions intermingled with subaerial environment. Recently, based on the presence of rhizoliths, and vertebrate trackways associated with the aeolian deposits, and the abrupt contact between the carbonate and the sand deposits, Mountney & Jagger (2004) and Mountney (2006) interpreted the Cedar Mesa Sandstone in the Neddles District as dry, wet and stabilizing systems under water-table control. This erg system is bounded to the west by a shallow-marine seaway (e.g. Blakey, 1988; 2008; Blakey *et al.*, 1988; Peterson, 1988; Lawton *et al.*, 2015) (Fig. 1B) and transitioned to sabkha deposits toward the southeast (Condon, 1997; Blakey, 1988; Langford & Chan, 1993; Taggart *et al.*, 2010). These sabkhas have recently been interpreted as saline lakes lacking marine influence (Pettigrew *et al.*, 2021).

In an earlier palaeogeographic interpretation of the Organ Rock Fm, Baars (1962, 1975) suggested this formation was deposited on a seaward-sloping coastal plain by streams, on floodplains and tidal flats, possibly with minimal marine reworking. Blakey (1979, 1980) suggested that some of these deposits were reworked by marine water over a broad flat profile. Stanesco *et al.* (2000) interpreted the Organ Rock Fm as a mixed fluvial and aeolian sediments dominated by braided channels in the proximal area (northeast), grading to meandering channels on a low-relief coastal plain, becoming dominated by aeolian deposits in the distal western part. Recently, Cain & Mountney (2009) re-interpreted the Organ Rock Fm as a semi-arid terminal fan system with sheet-floods and aeolian deposits dominating in the southwest distal part.

The lower part of the White Rim Sandstone is composed of sand-sheet or sabkha deposits characterised by algal laminations, wind-ripple strata, and small-scale cross-bedded, bioturbated intervals, breccia layers, adhesion ripples, and desiccation polygons (Huntoon & Chan, 1987; Kamola & Chan, 1988; Chan, 1989; Langford & Chan, 1989). Its upper part is composed of aeolian dunes intermittently flooded by marine water, attested by *Thalassinoides*, *Chondrites* burrows and glauconite grains (Steele, 1987). Its top is reworked by marine processes, indicated by characteristics such as symmetrical ripples, fluid escape features, and the presence of *Ophiomorpha* burrows (Orgill, 1971).

The Undivided Cutler Gp deposits are interpreted as alluvial fans, debris flows and proximal braided-stream deposits (Campbell, 1980; Mack & Rasmussen, 1984; Schultz, 1984; Dubiel *et al.*, 1996) with occurrence of aeolian deposits (Hême de Lacotte & Mountney, 2022). Sedimentation was influenced by contemporaneous growth of anticlinal structures, such as the Cane Creek anticline (Wengerd & Matheny, 1958) caused by movements of the deep Paradox Salt Fm (Venus *et al.*, 2015). The structures constituted barriers to the coarse sediments and explain the dramatic changes in thickness across the basin of the Undivided Culter Fm (Condon, 1997; Venus *et al.*, 2015). However, Moore *et al.* (2008) suggested that at the time of deposition of the Undivided Cutler Gp movement along the subsurface Uncompahgre fault had ceased. Moreover, the Undivided Cutler Gp is attributed to lacustrine-fluvial processes in a cold proglacial system (Soreghan *et al.*, 2009; Keiser *et al.*, 2015).

3. Methods

Five detailed sedimentological sections were measured and analysed across the Canyonlands National Park study area (Fig. 1). From north to south these sections are referred to as: Hurrah Pass (355 m; Figs. 3A, 4), Potash Road (382 m; Figs. 3B to D, 5), Lockhart Canyon (270 m; Figs. 3E to G, 6), Elephant Hill (Fig. 7, constituted of 2 sections, one in the recreation area, 122 m, Fig. 3H to J, and the other outside the Park, 215 m, Fig. 3K, L), and Cathedral Butte (225 m, Figs. 3M, 8). Thicknesses were measured using a 1.5 m Jacob's staff. The facies analyses include sedimentological structures, paleoflow measurements of hydraulic and aeolian deposits, i.e. azimuths of foresets of ripples, megaripples, sand dunes, and orientations of the axes of troughs seen in plan-view sections (not corrected for paleogeography), determination of the fossil content (marine fossils, paleoflora, and bioturbation), and were completed by 24 petrographic thin section analyses collected from the five measured sections (Figs. 4 to 8).

A terminology modified from Miall (1996) and Cain & Mountney (2009) is used to describe fluvial and aeolian deposits. From each measured section a sedimentological study of

a vertical depositional environment profile has been drawn that allows the recognition of genetic units. Architectural data compiled from a series of panels, from direct field measurements (around 10 for each section), from tracing of photomontage by classical methods or by drone acquisition in the Lockhart canyon area, show the lateral and vertical extent of the facies, the spatial arrangement of sets and strata and their bounding surfaces. From each section, the recognition of major surfaces, from panels and satellite images (Google Earth), as well as stratigraphic cycles, is used to perform high-resolution correlation at the scale of the studied area (Fig. 1). The correlation uses the principle of high-resolution sequence stratigraphy, based on the stacking pattern of the smallest stratigraphic units (Van Wagoner *et al.*, 1988) within a sedimentary succession (parasequences, Van Wagoner *et al.*, 1990; Mitchum & Van Wagoner, 1991, or genetic units, Cross, 1988; Cross *et al.*, 1993). By observing the stacking arrangement of genetic sequences, bounded by maximum flooding intervals, above and below, different scales of stratigraphic cycle can be identified. With increasing scale and duration, these stratigraphic cycles are termed genetic sequence sets, minor stratigraphic cycles, and major stratigraphic cycles.

To correlate the sections, it is necessary to define a reference surface, i.e. a horizon that represents the shortest interval of time that is recognizable in all 5 sections. In the Lockhart Canyon section, the youngest carbonate (86 m, in Fig. 6) at the top of the lower Cutler beds contains nautiloids, *Tainoceras sp.,* and other marine fossils, such as *Wilkingia* sp. and *Bellerophon*, corresponding to an early Permian fossil assemblage, and is attributed to the Shafer Limestone. This level is overlain by a clay facies with abundant shells of *Wilkingia* sp. in life position, located on top of the first cliff at Lockhart Canyon (Fig. 3F) and overlain by a layer with abundant wood fossils. This surface is easy to recognize in the landscape and was used as a correlation surface (on Google Earth images) at the scale of the study area (Supplementary Data Fig. 1). It is our reference level noted as D on the correlation charts (Figs. 3A, B, F, H, 4, 5, 6, 7). For the Elephant Hill sections, we walked on a benchmark surfaces, which allowed the correlation between the three Elephant Hill sections (noted 1 and 2, Fig. 7). Between Elephant Hill and Cathedral Butte sections another characterized surface noted E (Figs. 3I, M, 7, 8) has been drawn from Google Earth images (Supplementary Data Fig. 1). The top of the sections is defined by the Triassic unconformity. To the south of the studied area, i.e. Elephant Hill and Cathedral Butte sections (Figs. 7, 8), the level located below the unconformity is characterised by numerous well-preserved large stumps fossilized *in situ* and logs (noted respectively Pst and Pw, Supplementary Data Fig. 2E2, E3 and 3F3) documenting the occurrence of large trees growing here.

4. Facies association analysis

Sandstone facies are predominant within the Permian succession of Utah. They are associated with some conglomeratic and fine-grained facies. These facies, summarized in Table 1, are more or less bioturbated (Supplementary Data Fig. 3) or display pedogenic features (Supplementary Data Fig. 2). Facies associations are interpreted below and summarized in the Table 2.

4.1. Facies association E: Erg deposits

4.1.1 Description

This facies association (Fig. 9) is characterised by sandstones facies: AT, Ah, Ar (Table 1). Three facies associations are present (Table 2): E1 (facies AT and PR, Prmo, Fig. 9A, D, F), E2 (facies Ah, Ar; Fig. 9C, E) and E3 (facies Ar, Aa and PR; Fig. 9F, G). The E1 facies association is mainly composed of AT facies with foreset directions oriented to the southeast (Table 2). Two types of vertical root traces, up to 15 cm in diameter, and several metres long have been observed in the upper portion of some of the dunes: some root traces have preserved wood (named PRmo, Supplementary Data Fig. 2D1), and, in others generally thinner roots, the wood is absent (named PR, Supplementary Data Fig. 2C3). In other cases, the compound cosets has been colonised by burrowing organisms (Fig. 9J).

The petrographic analyses of these sandstones (Supplementary Data Fig. 4) show 85 to 90 %, monocrystalline quartz grains, glauconite, fragments of crinoids and foraminifers, and oolites (Supplementary Data Fig. 4). The cement is predominantly calcitic, however in rare instances it is siliceous.

4.1.2. Interpretation

Facies AT, which is the main constituent of the E1 facies association, is interpreted as aeolian dune (Tables 1, 2) with predominant wind ripples and avalanche features characterising the basal part of the dune (Langford & Chan, 1989; Veiga *et al.*, 2002). Large-scale convolutions are attributed to sand liquefaction during periods with high water table (Allen & Banks, 1972; Doe & Dott, 1980). In consequence, E1 corresponds to aeolian dune migration with paleowinds mostly from the northwest (Table 2). The vertical root traces with preserved wood (PRmo) observed are attributed to plants that have the capacity to produce very large, nearly vertically penetrating roots. At this time in Earth history, the most likely candidates are woody gymnosperms, perhaps some form of cordaitalean, conifer, or dicranophyll. Plants of this type have been reported from xeric, coastal settings of Late Pennsylvanian and early Permian age in New Mexico (Falcon-Lang *et al.*, 2011, 2015, 2016), thus in environments similar to those discussed here. Of course, there are other plant groups reported from water-stressed semi-arid to arid settings of Permian age, in addition to the woody coniferophytes. These include such plants as gigantopterids (e.g. Simon *et al.*, 2018a), supaioids (e.g. White, 1929; DiMichele *et al.*, 2007), comioids (e.g. Mamay *et al.*, 2009), or even certain callipterid peltasperms (e.g. Falcon-Lang *et al.*, 2015). In addition, it must be kept in mind that the parent plants of these roots may have belonged to a yet unknown group. The other root traces (PR) may simply be less mature versions of the larger roots, or could represent some other group of plants capable of tapping into deep water tables. There are no criteria, however, that clearly distinguish these roots, as a different biological taxon from the larger diameter roots. The difference between these two classes of roots may be simply a consequence of sediment built up around a much thinner living root. However, the paleosol above the dunes field is rarely preserved and only vertical root-traces indicate that a soil was once present above the sand dunes. The paleosols overlying aeolian dunes attest to a change to more humid conditions that allowed the development of plants such as cordaitaleans, or other drought-tolerant groups.

The aeolian dunes can also bioturbated by burrows attributed to *Diplocraterion*, *Planolites,* or animal bioturbation of indeterminate affinity (Fig. 9J; Supplementary Data Fig.

3A1, C1). The evidence of colonisation by marine burrowing organisms attests to periodic marine flooding episodes.

The E2 facies association (Table 2), consisting mainly of migrating wind ripples and traction deposition by high velocity winds (respectively Ar and Ah facies, Table 1), characterises either interdunes (Veiga *et al.*, 2002; Kocurek & Nielson, 1986) or aeolian sand-sheets where wind regime conditions and/or sand supply prevent the development of dunes (Kozureck & Nielson, 1986; Trewin, 1993).

Facies Aa and Ar are interbedded in the E3 facies association (Table 2). The adhesion structures are the result of dry, wind-blown sand sticking to a wet or damp surface (facies Aa, Table 1). E3 represents alternation of either dry and wet aeolian sand-sheets, or wet aeolian sand-sheets and interdunes (Hunter, 1977; Kocurek & Nielson, 1986). Root traces (PR) are sometimes present at the top of this facies association.

The occurrence of marine fossils together with glauconite within aeolian sandstones attests to reworking of coastal sands by wind as suggested by Loope (1981, 1984). However, for this author, these debris could have been transported over more than 800 km and do not prove an interaction with marine depositional environment (Loope, 1984).

4.2. Facies association F: Fluvial and alluvial plain deposits

4.2.1. Description

This facies association (Fig. 10) is characterised by conglomerates (facies Gm, Gt), sandstones (Sm, St, Sh, Shd, Std, Sr, SF), silty-clay (facies F, Fl) and heterolithic (facies SF, SFl) deposits (Table1). These facies occur together within four facies associations (Table 2): F1 (Fig. 10C), F2 (Fig. 10C, G), F3 (Fig. 10G, K, L) and FE (Fig. 10M).

The petrographic analyses of fluvial sandstones show a composition of 75% monocrystalline quartz grains with the remaining 25 % being a combination of biotite, muscovite, plagioclase, microcline, perthitic alkali feldspar, heavy minerals (zircon, tourmaline), and lithic fragments. The cement is predominantly calcitic with some iron oxides (Supplementary Data Fig. 4). Four facies associations are observed: F1, F2, F3 and FE (Table. 2).

4.2.2. Interpretation

F1 suggests deposition in braided rivers, consisting of isolated or stacked channel deposits composed of tractive deposits with mainly 3D megaripple bedding, and unimodal, low dispersive mainly southwest-trending paleocurrents (Fig. 2). Well-exposed trunks of trees, conifers or cordaitaleans (Pw; Supplementary Data Fig. 2F4), are observed interbedded within braided river deposits. The rivers must have been large enough to transport logs without destroying them before fossilization and, due to their large size, a long distance of transport is unlikely (e.g. Wyżga *et al.*, 2017). The occurrence of big trees implies that the water table

were at least seasonally shallow. Trees with large trunks were almost certainly growing in areas that experienced wet-dry seasonality with the dry season predominating.

F2 is characteristic of unchannelled streamflows attributed to sheet-floods in the distal braid plain (Miall, 1996), consisting mainly of planar beds deposited by density flow and tractive current.

F3 is typical of alluvial plains under semi-arid climatic conditions, with waning floods, overbanks, mud-cracks, and pedogenic carbonate nodules (Hasiotis & Bourke, 2006; Hasiotis *et al.*, 2007).

Within F2 and F3 facies associations, the root traces associated with carbonate nodules (Prn) are interpreted as having formed under arid conditions with intermittent heavy rainfall (e.g. Retallack, 1988; Colson & Cojan, 1996). The irregular beds composed of carbonate nodules, frequently observed below Pr or Prn, result from the mixing of fresh and brine waters, which infiltrates the phreatic zone during periods of high evaporation (Colson & Cojan, 1996).

FE, rarely observed, composed of planar beds, is characterised by deflation lags within stream flood deposits and aeolian deposits (Clemmensen & Abrahamsen, 1983; Langford & Chan, 1989). The lack of both channels and true classical clayey floodplain facies indicates ephemeral floods with numerous channels and a high lateral migration rate within an arid alluvial plain (Bourquin *et al.*, 2009).

The petrographic analyses indicate basement sources.

4.3. Facies association C: Coastal marine deposits

4.3.1. Description

Facies association C (Fig. 11) is mainly characterised by (Table1): bioturbated sandstones (Stb, Shb, Sb, Msig, Srw, SFb), or siltstones (Fb, Flb), and comprises some bioclastic carbonates (Cf), sandstones (Stf, Sbf), and conglomerates that occasionally contain marine bioclasts (Gm, Gt). Three facies associations are observed (Table 2, Fig. 11N): C1, C2, and C3.

4.3.2. Interpretation

C1 is ascribed to distributary mouth-bars and unconfined flow with paleocurrents in the channelled deposits indicating currents predominantly toward the southwest and occasionally toward the southeast (Table 2). The bioturbation is attributed to *Diplocraterion* and *Planolites* (Fig. 11B, Supplementary Data Fig. 3A2, C2) that confirm marine depositional environment. The southeast paleocurrent is interpreted as the result of reworking of the sediment by longshore currents.

C2 characterises supra- to intertidal deposits with storm wash-over deposits. The trough cross-bedding with bipolar paleocurrent directions (or tidal bundles) of the Msig facies is attributed to tidal bars deposited in the subtidal zone or within tidal channels. The occasionally encountered low-angle, horizontally laminated to cross-bedded bioclastic sands and sandy limestones reflect foreshore deposits dominated by storm deposits on a supratidal shelf. The ichnofacies are mainly *Scolocia*-like and *Thalassinoides* (Supplementary Data Fig. 3D, E), rarely *Psilonichnus* (Supplementary Data Fig. 3F).

C3 bioturbated sandstone with an overprint of paleosol development is interpreted to have been deposited at the intersection between the tidal flat and terrestrial environment, corresponding to marsh or coastal plain settings. The indeterminate bioturbation of both Shb facies, with horizontal to subhorizontal lamination and rare fluid escape structures, and Sb facies correspond to sheet-flood deposits formed at relatively shallow depths on the top of mouth-bars (e.g. Pollard *et al.*, 1982; Marshall, 2000; Hinds *et al.*, 2004; Bourquin *et al.*, 2010).

4.4. Facies association S: Subtidal to shoreface/offshore deposits

4.4.1. Description

Facies association S is mainly composed of (Table 1): very fine- to medium-grained sand (ST, Sb, Shb, Srb, Srw Sm, Sr), heterolithic facies (SFb, SFl), and some fine-grained facies (Fl, Flb, F, Fb). Two facies associations are distinguishable, S1 and S2 (Table 2, Fig. 12).

The petrographic analyses of these sandstones (Supplementary Data Fig. 4) show 85 to 90 %, monocrystalline quartz grains. Glauconite, fragments of crinoids and foraminifers, and oolites, also are present. The cement is predominantly calcitic but there are rare samples in which it is dolomitic.

4.4.2. Interpretation

The organisms responsible for bioturbation are either undetermined or assignable to the ichnogenera *Planolites*, *Palaeophycus,* or rarely crustacean (Tables 1, 2, Supplementary Data Fig. 3A, B). The presence of wave ripples and marine bioturbation support the interpretation of a marine depositional environment. These sandstone facies show more mature material than fluvial deposits with reworked marine-fossils.

S1 corresponds to offshore bars or detached shoreface dune deposits (Plint, 2010), with a longshore current oriented to the southeast (Table 2). The vertical root traces of several metres length (PR, PRmo) occasionally observed at the top of compound cosets of longshore dunes, attributable either to cordaitaleans, conifers, or indeterminate vegetation (see above), are indicative of periods of subaerial exposure after the formation of these hydraulic dunes. However, the paleosol above the dunes is rarely preserved and only the vertical root-traces indicate that a soil was once present above the sand dunes. The soil overlying the subaqueous dunes attest to an abrupt transition to terrestrial conditions.

S2 (Table 2) represents a subtidal environment that evolved vertically to episodic subaerial exposures. It is mainly characterised by current-ripples, oscillatory-ripples, some horizontal bedding and occasionally root traces (Pr, PR).

5. Depositional environments and high-resolution stratigraphic cycles

5.1 Late Pennsylvanian to early Permian depositional environments

The current study finds that marine influence is a component of all three Late Pennsylvanian to early Permian formations in the Paradox Basin of Utah. Previous recent studies of these formations overestimated the occurrence of aeolian dunes and the underestimated longshore bar sediments, with obvious and major implications for the reconstruction of the regional landscape. Longshore bars and aeolian dunes were not distinguished because many features are similar in a cursory examination. Additionally, the foreset dip azimuth is similar, both facies being strongly wind-influenced, resulting in generally the same southeast dip orientation (Fig. 13A). Only detailed facies study allows the differentiation of these sedimentary bodies, with aeolian dunes having typical grain flow and grain fall strata, and with wind ripples, whereas longshore bars are affected by marine bioturbation in their entire body (not only in the upper part of their preserved foresets) and are characterised by bottomsets interdigitated with silts (Fig. 13A). In consequence, a depositional model for the entire Permian succession of the studied area (Fig. 1), i.e. from lower Cutler beds to White Rim Fm, based on the above facies analysis is proposed Figure 14.

5.2 Sequence stratigraphic framework

Using surfaces (Supplementary Data Fig. 1), as anchor horizons, a regional correlation between the five reference sections is possible. The repetition of changing depositional environments through time in the measured section allows to define high resolution stratigraphic cycle, i.e. genetic sequences (Fig. 15) that will be discussed below for each formation. Three types of stratigraphic surfaces can be defined: sand-drift, flooding and maximum flooding surfaces. The criteria for defining allocyclic events are based on the abrupt change of facies across these surfaces and their lateral continuity on a large geographic scale.

5.2.1 Lower Cutler beds

The lower Cutler beds Fm (Figs. 4 to 7) is composed of mixed marine and continental deposits (Fig. 16A, B). The shoreface deposits represent the predominant facies association, up to 15 m thick, composed of often well-developed stacked longshore bars. These bars can be intensely bioturbated (*Planolites, Palaeophycus*, crustacean burrows, or indeterminate bioturbation, Supplementary Data Fig. 3). At the top of these bars, root traces are occasionally observed (Pr, PR). Within the Hurrah Pass section large diameter, long rhizoliths with preserved wood, PRmo, are present, attributable to a tree, likely cordaitaleans or conifers, although, as noted earlier, there certainly are other possibilities (Supplementary Data Fig.

2D2, D3). The coastal facies are characterised by mouth-bars and tidal flats, with various ichnogenre attributed to *Psilonichus, Diplocraterion, Planolites, Thalassinoides, Scolocia*-like, and *Bichordites*-like (Table 2). The braided rivers have large trunks of trees, probably conifers or cordaitaleans, that were living on the braid-plain where there was at least some kind of wet season. Such trunks are particularly well-exposed in the basal part of the Potash road section (around 6 m, Fig. 4; Supplementary Data Fig. 2F4). In all sections, the aeolian deposits are well-developed in the upper part of lower Cutler beds where 6-m thick stacked aeolian dune or sand-sheet deposits occur (Fig. 16A, B). Fossil wood and rhizoliths also occur in the youngest bioclastic deposits that contain marine macrofauna at the top of lower Cutler beds representing the reference level for correlation D (Fig. 3; Supplementary Data Fig. 1). In the Potash road section, it is correlative to the cornaline rhizolith beds (Supplementary Data Fig. 2E1) that overlie bioclastic limestones with macrofauna (at around 163 m, Fig. 5) and are, in turn, overlain by coarse-grained (Gm facies) mouth-bar deposits that contain macrofauna remains. This correlative bed is present at 90 m in the Lockhart Canyon section (Fig. 5; Fig. 16A, B) that has abundant silicified wood clasts. This bed is bounded below by a fossiliferous bed containing large bivalves (*Wilkingia* sp.) and above by mouth-bar deposits. The wood fragments are attributed to coniferophyte branches up to 20 cm in diameter (Supplementary Data Fig. 2F2).

These depositional environments dominated by shoreface and fluvial deposits allow to define the genetic sequence type 1 (Fig. 15A). The maximum flooding episode is located at the base of longshore bar deposits (S1 facies association, Fig. 15A). The progradational phase is characterised by a change from subtidal environments with longshore bar (S1, S2) and tidal flat (C2), coastal plain (C3), and mouth-bar deposits (C1) to fluvial (channelled, F1, or unchannelled streamflows, F2) and alluvial plain (F3) deposits. The paleosol development indicated by root traces is observed within the coastal (C3) and the alluvial (F3) deposits. The retrogradational phase is marked by alluvial plain deposits (F3), dominated by unchannelled deposits (F2) with occasional channelled (F1), overlain by mouth bar (C1) and coastal plain deposits (C3). This sequence is rarely complete (Fig. 12H) and frequently truncated (Fig. 11N), i.e. the retrogradational phase is rarely recorded. The base of this sequence may also be lacking or truncated, with the maximum flooding episodes having been recorded within mouth-bar and coastal plain deposits. A second type of genetic sequence (Type 2, Fig. 15B) with preservation of aeolian deposits (E1, E2 and E3) can be also observed. They are superposed on the fluvial deposits (F1, F2, F3 or FE) and terminate the progradational phase (Fig. 15B, 16 A, B). From the base of the section to the reference surface D, 14 genetic units have been defined (noted a and 1 to 13, Figs. 1 to 8 and 17). They can be grouped in 5 minor cycles (notes I to V, Figs. 1 to 8 and 17).

These depositional environments have been previously described by Terrell (1972) for the lower Cutler beds, with marine bars and aeolian dunes. This precursory work described nearly cyclic transitional marine to non-marine carbonate and clastic rocks with clastic debris from adjacent Uncompahgre Highland and the accompanying retreat of the sea. Jordan & Mountney (2010) defined a depositional model with only shallow marine facies, all the sandstones dunes being described as aeolian dunes. Jordan & Mountney (2012) and Wakefield & Mountney (2013) considered at least 12 marine transgressive-regressive sequences, the fluvial deposits being preserved in incised-valley.

5.2.2. Cedar Mesa Sandstone

The Cedar Mesa Sandstones since Loope (1981) is classically considered as exclusively continental, dominantly of aeolian dune origin, with intervening deposits of dry, damp and wet interdune, restricted lacustrine pond, inland (i.e. continental) sabkha, and fluvial origins (e.g. Mountney & Jagger, 2004; Mountney, 2006; Pettegrew et al., 2021). In the studied part of the basin, the Cedar Mesa Sandstone is composed primarily of aeolian dune, but shoreface deposits were also identified (Figs. 4 to 8). The longshore bars (Fig. 16C, D) are less developed than in the lower Cutler beds and do not exceed 9 m in thickness (Figs. 4 to 8). Few fluvial or mouth-bar deposits are observed within the Cedar Mesa Sandstone (Fig. 16D). Large rhizoliths are preserved in the upper part of the compound cosets of longshore bars or aeolian dunes. In the Hurrah Pass section, at the base of this formation (Fig. 4), large, long permineralized roots, PRmo, mostly likely attributable to coniferophytes (Supplementary Data Fig. 2D1), are present in aeolian dunes. Above the 200-m level (Fig. 4), the rhizoliths lack permineralized wood and are thinner (PR and Pr); there are, therefore, no criteria clearly demonstrating that root size is not simply a consequence of sediment built up around a much thinner root. At Elephant Hill (Figs. 7) and Cathedral Butte (Fig. 8), the root traces are devoid of organics and are simply discolorations of the sediment (Pr, PR).

The genetic sequence type in the Cedar Mesa Sandstone is similar to the one of the upper part of the lower Cutler beds (Type 2, Fig. 15B). However, the progradational phase is rarely complete and some facies are missing (Figs. 12I, 15C, D), implying occasionally an abrupt transition from longshore bar to aeolian dune facies, sometimes underlain by root traces (Fig. 15E), whereas the retrogradational phase is rarely preserved (Fig. 15C, E, F). When it preserved, the retrogradational phase is marked by sediments recording aeolian sand-sheet (E3-E2-FE), alluvial (F3, F2, F1, FE), mouth bar (C1) and coastal environments (C3). The aeolian dune is truncated (MRS) and marked by root traces that indicate the presence of a paleosol that stabilized the dune surface thus also contributing to dune preservation (Fig. 15B). In genetic units lacking retrograde deposits, the retrogradational phase is marked only by an abrupt transition from aeolian dune to longshore bar, occasionally underlain by root traces, especially within the Cedar Mesa Sandstone (Fig. 15E), or, in some cases, by evidence of colonisation by organisms that burrow vertically into the substrate (Figs. 9J, 15F). As a consequence, large stacked sandstone bars with the same foreset orientation are preserved, the longshore currents and paleowind having similar orientations towards the southeast (Fig. 13B).

These high-resolution cycles are observed for the first time throughout this formation, and in continuity with the lower Cutler beds. From the surface D, 17 genetic units have been defined (noted 14 to 30, Figs. 1 to 8 and 17). They can be grouped in 6 minor cycles (noted VI to XI, Figs. 1 to 8 and 17).

Loope (1984) considered that Cedar Mesa Fm intertongues with marine carbonate only to the northwest and interpreted all the crossbedded sandstone in Canyonland national Park as aeolian in origin. This view contradicted interpretations by earlier authors and especially with Mark (1979), who considered longshore and aeolian bars. In this area, Loope (1985) interpreted the thin limestones and mudstones as probably lacustrine in origin, and he considered 40 flat-topped aeolian sand bodies, overlain by rhizoliths and burrows. The further studies propose high-resolution stratigraphic architecture at reservoir scale (i.e. outcrop) and considered fluvial-aeolian or sabkha-aeolian-fluvial interaction (e.g. Targaart et al, 2010; Mountney, 2012; Pettigrew *et al.*, 2021; Hême de Lacotte & Mountney, 2022).

555 5.2.3. Organ Rock Formation

556 The Organ Rock Fm is classically considered as mixed fluvial and aeolian and has been
557 described as terminal alluvial fan system (Stanesco et al., 2000). However, our study shows
558 that the Organ Rock Fm (Figs. 4 to 6) is mainly characterised by fluvial and mouth-bar
559 deposits associated with coastal or shoreface environments (Fig. 9H). Aeolian deposits are
560 occasional to the north (i.e. Hurrah Pass, Potash Road and Lockhart Canyon sections) and
561 more developed to south (Elephant Hill and Cathedral Butte sections). The fluvial deposits
562 consist of southwest oriented braided rivers and unchannelled stream flows (sheet-flood
563 deposits), with a few intercalated floodplain deposits. The mouth-bar paleocurrents indicate a
564 flow direction from the southwest to the southeast. The shoreface deposits are stacked
565 longshore bars, less than 10 m thick (Figs. 4, 6, 9H to I). At Lockhart Canyon (Fig. 5), only
566 the lower part of the Organ Rock Fm is observed, and shoreface deposits are absent. Within
567 this formation, the vertical root traces are similar to those observed in the upper part of the
568 Cedar Mesa Sandstone (long thinner root traces without organic matter preserved).

569 In the Organ Rock Fm, 8 genetic sequences (noted 31 to 38, Figs. 1 to 8 and 17) are
570 different between the north and the south, where they differ by the absence (15B) or presence
571 (Fig. 15 A) of aeolian deposits, respectively. The main difference with genetic sequences of
572 the lower Cutler beds is in the more developed fluvial deposits (especially at Potash road
573 section), and with those of the Cedar Mesa Fm in the more developed fluvial (Elephant Hill
574 section) or marine deposits (Cathedral Butte section). The genetic units can be grouped in 4
575 minor cycles (noted XII to XV, Figs. 1 to 8 and 17).

576 Cain & Mountney (2009) correlated five large-scale finning upward cycles ending by
577 aeolian deposits, below the Triassic unconformity. The upper part of their studied series, with
578 well-developed aeolian facies could correspond to the White Rim Fm. Moreover, Hême de
579 Lacotte and Mountney (2022) proposed a model of architectural relationships for these
580 fluvial-aeolian deposits.

581

582 5.2.4. White Rim Sandstone

583 The White Rim Sandstone is observed at the top of the sections with around 25 m
584 preserved strata (Figs. 3D, 5, 7, 8). In this part of the basin, this formation is mainly
585 characterized by fluvial, mouth bar facies and aeolian dunes abruptly and unconformably
586 overlain by Triassic deposits (Fig. 9F). In consequence, only 2 genetic sequences are partially
587 observed in each section (noted 39-40, Figs. 1 to 8 and 17) that characterized the end of the
588 minor cycle XV (Figs. 1 to 8 and 17).

589 In the northeastern part of the Paradox Basin, NW of Moab, Lawton et al. (2015), also
590 observe two aeolian deposits separated by fluvial environment within White Rim Sandstone.
591 The relative important thickness of this formation in their study, around 170 m, is attributed to
592 high subsidence rate dues to salt diapirism that occur in this part of the basin (Lawton et al.,
593 2015).

594

595 5.2.5 Stratigraphic surfaces

596

5.2.5.1. Sand-drift surface

The sand-drift surfaces (SDS, Fig. 15B, C, D, E, F) characterise the different types of erosional and depositional contacts between water-lain and wind-driven processes (Clemmensen & Tirsgaard, 1990). SDSs are formed by subaerial removal of previously deposited subaqueous sediments, and form an important bounding surface that represents a significant shift in processes controlling sediment transport. The formation of water-lain deposits predating the accumulation of aeolian deposits, controlled by the water-table position, has previously been documented in other aeolian successions, in coastal marine environments (e.g. Fryberger et al., 1984; Blakey, 1996; Blanchard *et al.*, 2016), or in endoreic basins (e.g. Veiga *et al.*, 2002; Bourquin *et al.*, 2009). After the development of a sand-drift surface, aeolian sand accumulation indicates a period of absence of fluvial sediment supply and is either assumed to express progradation within a terrestrial environment (Bourquin *et al.*, 2009) or the latter part of lowstands system tracts within marine coastal environments (Blanchard *et al.*, 2016). This indicates that the aeolian sediment availability reached a peak during progradation, but the preservation is permitted by the creation of the accommodation space. Therefore, the SDSs are not synchronous surfaces and only preserve a single period during the end of progradation without fluvial sediment supply and the beginning of water table rise, which allows the preservation of aeolian deposits (Fig. 15B to E).

5.2.5.2. Supersurfaces: deflation or flood surfaces

Contact surfaces between aeolian dunes and the overlying lithologies are often sharp. These sharp surfaces are known as supersurfaces (Kocurek, 1988) and result from climatic and relative sea-level changes (e.g. Loope, 1984; Mountney, 2006, Bourquin *et al.*, 2009; Blanchard *et al.*, 2016).

In coastal settings, they represent a period of marine erosion resulting in a deflation surface formed prior to a transgression (Chan & Kocurek, 1988). The deflationary supersurface results from a shutdown of sedimentary source material caused by flooding occurring upwind of the erg margin, or by an increase of vegetation cover, or rise of the water level (Kocurek & Havlom, 1993; Mountney, 2012).

Flooding surfaces are defined by the flooding of aeolian deposits, independent of their size and lateral extent (Clemmensen & Tirsgaard, 1990; Fryberger, 1993; Langford and Chan, 1988). In some instances, the preservation of an aeolian dune can be caused only by pure marine flooding, which also induced the generation of that supersurface (Blanchard *et al.*, 2016).

In our study area, these two types of supersurfaces can be observed (FS and MRS). The flooding surface (FS, Fig. 15B) marks an increase in fluvially transported sediment but does not represent a stratigraphic surface at the scale of the genetic unit (Bourquin *et al.*, 2009). In fact, the transition from progradational to retrogradation phases that represent the stratigraphic surface is located at the top of the aeolian deposits. Blanchard *et al.* (2016) consider these surfaces equivalent to the maximum regressive surfaces (MRS; Helland-Hansen & Martinsen, 1986; Catuneanu *et al.*, 2009). The MRS corresponds to the beginning of deflationary episode during which the dune field was colonised by vegetation (Fig. 15B). In other cases, the aeolian deposits are overlain by shoreface facies or coastal deposits, and the top of the aeolian

dune can be colonised by burrowing marine organisms (Fig. 15F). If only root traces are observed at the top of aeolian dunes, the presence of a subsequently eroded paleosol is indicated (Fig. 15E). In this case, the retrogradation phase is not preserved; rather, the MRS and the maximum flooding surface (MFS) represent the same surface (Fig. 15E). To conclude, the top of the aeolian dune field is marked by supersurfaces representing either time hiatuses (marked by root traces, Fig. 15E) or direct flooding episodes (burrowed by organisms, Fig. 15F).

5.2.5.3. Maximum flooding surface

The maximum flooding surface (MFS) is interpreted to be marine flooding surface (e.g. Posamentier & Vail, 1988; Van Wagoner et al., 1988). However, such surfaces have been recognized in terrestrial environments without any marine influence (e.g. Legarreta *et al.*, 1993; Olsen, 1995; Currie, 1997; Bourquin *et al.*, 1998, 2009). In this case, these surfaces mark the transition from retrogradational to progradational phases, characterised by extensive floodplain or lake sediments.

Within the studied area, the more distal facies are characterised by shoreface deposits, i.e. longshore bar or subtidal deposits. The MFS is located either at the base of the longshore bar or within subtidal facies. Its lateral equivalent corresponds to well-developed coastal plain deposits (Fig. 15).

5.2.5.4. Sequence boundary

In continental settings, the period of progradation is characterised by low sediment preservation. Firstly, the terrestrial surface over which progradation occurs often is marked by well-developed paleosols. Furthermore, as the progradational phase accelerates, it is marked by an increase of sediment supply associated with fluvial incision, and lag deposits or amalgamated fluvial channel beds (e.g. Bourquin *et al.*, 1998, 2009). These specific deposits can be present or absent. When they are present, their base characterises the sequence boundary surface (SB), which is diachronous across the basin. In this study, with mixed marine and terrestrial depositional environments, the increase of sediment supply is greatest at the base of mouth-bars or at the base of fluvial deposits (Fig. 15A). When aeolian deposits are preserved, the SB is clearly delineated at the base of the fluvial or mouth-bar deposits below the aeolian dunes (Fig. 15B). This SB can coincide with the SDS surface (Fig. 15C, D, E).

6. Landscape reconstruction

For the first time, this study shows the general evolution of Permian environments, i.e. the lower Cutler beds, Cedar Mesa Sandstone, Organ Rock Fm and White Rim Sandstone, in the Paradox Basin (Fig. 17). The general evolution of this area allows two major cycles to be defined (noted M1 and M2, fig. 17). From the base of the sections to the MRS of the cycle XI, the major progradational phase of the M1 cycle took place, marked by the evolution from shoreface deposits to a broad aeolian dune field. The retrogradational phase of the M1 cycle is mainly characterised by marine, and alluvial plain deposits, up to a widespread marine episode that defines a major MFS. The M2 cycle is characterised by a vertical evolution to

683 mouth-bar and fluvial facies in the northern part and to fluvial and aeolian deposits in the
684 southern part (cycles XV). This progradational phase is truncated by the Triassic base
685 unconformity in this part of the basin.

686 Landscape evolution of the Paradox Basin, based on the correlations, is presented in
687 Figure 18. Three steps of development are recognized (Fig. 18 A to C).

688 The first step (cycle I to V, i.e. lower part of the M1 cycle or lower Cutler beds; Figs.
689 17, 18A), is mainly characterised by a shoreface environment, with longshore bar, braided
690 river, and mouth-bar deposits. The occurrence of large root traces and preserved wood (trunk
691 up to 18 m long at the base of the section) and branches of up to 30 cm in diameter at the base
692 of this first step, transported by braided rivers indicates that trees lived in the drainage basin.
693 A variety of vegetation, likely including trees grew on the braid-plains where ground water
694 levels were at least seasonally shallow during a wet season. The development of an aeolian
695 dune field begins in the upper part of this first step (cycles IV and V, Fig. 16).

696 In a second step, (sequences VI to XI, i.e. end of progradation of the M1 cycle or Cedar
697 Mesa Sandstone, Figs. 17, 18B), broad aeolian dune fields are present across the entire study
698 area (i.e. Cedar Mesa Sandstone, Fig. 17). The dune fields overlie rooted shoreface deposits
699 (surface D). Large and long root traces with preserved wood are also present in the top of the
700 aeolian dunes and are tentatively attributed to woody plant, possibly cordaitaleans or conifers,
701 recognizing that there are other possibilities, including plants we know little or nothing of as
702 macrofossils. This feature indicates episodes of wet conditions during which the area was
703 colonised by vegetation, followed by periods with dry conditions accompanied by the
704 development of aeolian features. The sand of the aeolian dunes is slightly finer than that of the
705 subaqueous dunes. The aeolian dunes contain grains attributable to marine fossil remains,
706 such as foraminifers, that demonstrate remobilization of marine sands.

707 A third step (cycle XII to XIV, i.e. end of retrogradational phase of the M2, i.e. Organ
708 Rock Fm; Figs. 17, 18C) is characterised by decreasing aeolian dune field deposits, shoreface
709 environment, and mainly fluvial deposits. Within the southern part, the aeolian environments
710 are interbedded with shoreface deposits, with few longshore bars, whereas in the northern
711 part, fluvial with some mouth-bar deposits are more developed occasionally overlain by
712 aeolian deposits. These features imply a decrease of wind-driven sand mobilisation and an
713 increase of fluvial input in the basin, which will accelerate during the second major
714 progradational phase of the M2 cycle.

715

716 ## 7. Discussion

717 A high-resolution correlation of the entire Permian stratigraphic succession in the
718 Canyonlands National Park (Fig. 1) allows discussion of landscape evolution in time and
719 space. The proposed scenario documents an interaction between aeolian dune fields,
720 shoreface, mouth-bar and fluvial deposits (Figs. 17, 18). Previous studies have been focused
721 on one formation and therefore missed the significance of a robust regional analysis of
722 sedimentary filling of the basin.

723

724 ### 7.1. Significance of cyclicity

Within the Late Pennsylvanian to early Permian succession studied herein, as preserved in the Paradox Basin, there are 40 genetic units within 15 minor stratigraphic cycles. The sedimentary record reflects both relative sea-level fluctuations and the variability of sediment supply resulting from the changing amount of precipitation in the source area. The Uncompahgre Highlands were the source area (Fig. 1) from which the derived sediment was deposited primarily on fluvial floodplains and in coastal mouth-bar (Lawton et al., 2021). Tidal influences and longshore bars are less dominant vertically and give way to less marine influenced sediments higher in the succession. Aeolian deposits, more prevalent up section, are more common in the southern part of the study area than in the north where they are interdigitated within fluvial deposits.

For the lower Cutler beds, Jordan & Mountney (2012) and Wakefield & Mountney (2013) considered the hypothesis that both climate and eustasy were interdependent and probably responding to a glacio-eustatic driving mechanism as suggested by (Rankey, 1997; Soreghan et al., 2002a). For the Cedar Mesa Sandstone, previous workers (e.g. Loope 1984, 1985; Langford & Chan, 1989; Mountney & Jagger, 2004; Mountney, 2006; Taggart et al., 2010; Pettigrew *et al.*, 2021) did not consider marine influence, thus they envisioned accumulation and preservation induced only by slow rises of the relative water-table due to climate variations driven by Milankovitch-type cyclicity. For the Organ Rock Fm, an evolution to progradational alluvial fan and its downstream passage to aeolian-dominated deposits have been put forward (Stanesco et al., 2000; Cain & Mountney, 2009, 2011; Hême de Lacotte & Mountney, 2022). The White Rim Sandstone records a coastal aeolian erg system with marine transgression (Huntoon & Chan, 1987; Kamola & Chan, 1988; Chan, 1989; Langford & Chan, 1989).

Wanless & Shepard (1936) had suggested glacio-eustatic control on late Palaeozoic cyclicity, but the magnitude of each sea-level fluctuation is still subject to many uncertainties (e.g. Rygel *et al.*, 2008). Rygel *et al.* (2008) pointed out that large-scale fluctuations (100-120 m) were probably restricted to the very Late Pennsylvanian-Cisuralian times, when ice sheet extent reached a peak during the LPIA. Recently, Blanchard *et al.* (2016) proposed a sequence stratigraphic framework for mixed aeolian, coastal, and marine environments in the Pennsylvanian of western Pangea and suggested that the accumulation of aeolian dunes took place during the latter part of the lowstands system tract and not during the sea-level fall as initially suggested by Carr-Crabaugh & Dunn (1996).

Two types of fluvial deposits are recognized (Fig. 15B). The first, above the longshore dunes in a progradational setting occurs at the end of sea-level fall, and is overlain by aeolian dune fields; the second, which occur during the sea-level rise, is above the aeolian dune fields, i.e. in a retrogradational setting (Fig. 19). Aeolian erg construction occurs during lowstands system tract when sediment availability is at a maximum being preserved during the early stage of transgression (Fig. 19). Aeolian dune fields are sharply truncated marking an MRS. In the southern part of the basin, where no non-marine facies are recognized, the MRSs and MFSs are combined (Fig. 15E). Two episodes of well-developed paleosols occur (Fig. 19): the first during the regression, at the beginning of the sea-level fall, and the second at the end of lowstands, during acceleration of the transgression.

Loope (1985) considered duration of the tabular genetic units (tabular aeolian sand bodies top by plane bedding with abundant roots and burrows) of around 400,000 years, where diastems present much more time than the rock themselves. In the equatorial terrestrial Pangea context, Cecil *et al.* (2014) suggest that a full cycle may have been completed in

771 approximately 100,000 years and these shorter cycles are superimposed on longer, 10^6 yr,
772 intervals of global warming and cooling, and those on a still longer-term trend of increasing
773 equatorial aridity. Moreover, some authors also indicate that the cyclothem record
774 precipitation variability on timescales shorter than the 100–400 kyr periodicities (e.g.
775 Olszewski and Patzkowsky, 2003; Tabor and Poulsen, 2008; Soreghan et al., 2014a,b). As the
776 age of the formations is unconstrained and the top is eroded by an unconformity (Figs. 2, 17),
777 it is very difficult to estimate the full duration of the preserved deposits. Knowing that it is
778 possible that some sequences are absent or stacked, only correlation to the northwest with
779 marine deposits would allow a more detailed discussion of the duration of this series.

780 Based on our observations, the following scenario is proposed to account for the
781 observed genetic units in the coastal environment of the central Pangean equatorial region
782 during Late Pennsylvanian to the early Permian (Fig. 20). This scenario takes into
783 consideration sea-level variation, the climate variation, which controls sediment supply and
784 vegetation cover will be discussed in the next step.

785 *Stage 1: Highstand system tract, maximum sea-level, end of interglacial phase*

786 In coastal environment, the tidal, subtidal and longshore bars are well preserved. The
787 vegetation cover limits the erosion of the hinterland, also reducing the sediment supply into
788 the basin and favouring fluvial aggradation.

789 *Stage 2: End of highstand, beginning of sea-level fall, beginning of glacial phase*

790 Fluvial sediment supply decreases and vegetation fixes alluvial and coastal deposits. In the
791 coastal environment, tidal and coastal deposits dominate the stratigraphic record with paleosol
792 (root traces or carbonate nodules) development in the terrestrial domain. The presence of
793 vegetation and its accompanying roots strongly limits erosion and thus sediment transport.

794 *Stage 3: Lowstands, minimum sea-level, glacial phase*

795 As sea-level falls, the terrestrial surface emerges with high sediment supply favouring fluvial
796 incisions, amalgamated channel belts, and progradation of mouth-bar deposits. During
797 lowstands, aeolian dunes start to be present but are very little preserved. This model differs
798 from those of Wakefield & Mountney (2013) where all the large-scale crossbedded
799 sandstones are considered as aeolian deposits subsequently incised by fluvial deposits at the
800 beginning of the falling stage

801 *Stage 4: End of lowstands, beginning of sea-level rise, transition to interglacial stage*

802 The fluvial sediment supply decreased, limiting fluvial erosion and allowing maximum
803 migration of aeolian dunes. The beginning of sea-level rise allows aeolian dune preservation.
804 This model is in accordance with those of Loope (1985) that considered aeolian preservation
805 during lowstands.

806 *Stage 5: Beginning of the transgressive system tract (TST), beginning of the interglacial stage*

807 For the aeolian dunes near the seashore, the beginning of the transgression is recorded at the
808 top of some aeolian dunes where marine animal bioturbation (burrows) is observed.
809 Landward, vegetational growth, as indicated by the rhizoliths, stabilizes the arid alluvial plain
810 and aeolian dunes.

Stage 6: TST - interglacial stage

In the coastal environment, the sediments are rarely preserved and mainly characterised by limited aeolian sand sheets and fluvial deposits. Semi-arid conditions are indicated by the presence of calcretes in paleosols and aeolian deposits.

7.2. Palaeoclimate implications

The aeolian deposit preservation occur the end of lowstands and in consequence at the end of the glacial phase. Strong linkages exist between global climate, ice volume, sea-level, and environmental conditions, with global and regional conditions greatly impacting vegetational change in the late Carboniferous and early Permian glacial world (e.g. Cecil *et al.*, 2014; DiMichele, 2014). However, the interpretation of climate differs according to the authors: either tropical climate is considered during glacial intervals as humid, i.e. wetter and less seasonal precipitation (e.g. Cecil et al., 2003, 2014; Eros et al., 2012) or as arid, i.e. drier and more seasonal precipitation (e.g. Rankey, 1997; Olszewski and Patzkowsky, 2003; Soreghan et al., 2008; Jordan and Mountney, 2012; Wakefield & Mountney, 2013), than during interglacial intervals.

In the central Pangean equatorial regions, coal and organic-rich shales occur in cyclic sequences, thus Cecil *et al.* (2014) and DiMichele (2014) conclude that the maximum rainfall and the minimum seasonality occurred during glacial maxima and thus sea-level lowstands. In craton interior, coal preservation occurs when equatorial rainfall exceeds evapotranspiration (Cecil *et al.*, 2014). Initiation of ice-sheet build-up progressively increases precipitation and decreases seasonality in the equatorial regions, which resulted in more vegetation (wetland forest) in all topographic areas surrounding a basin (Cecil *et al.*, 2014). During the early transgression (end of glacial phase), climate began a shift to seasonal, subhumid (Cecil et al., 2003) that reduced vegetation density on the landscape (Cecil *et al.*, 2014). As a consequence, in this equatorial coastal domain, the aeolian deposits reflect a reduction of vegetation that implies greater erosion and is probably also related to the onset of a more extensive seasonal migration of the Intertropical Convergence Zone (ITCZ) with higher wind velocities (e.g. Tabor & Poulsen, 2008).

Some climate simulations of tropical climate supported the hypothesis of dryer climate during glacial interval and consider the effects of glaciating the equatorial mountains (e.g. Heavens *et al.*, 2015). For these authors, this interval corresponds to strong winds caused by glaciation of the Central Pangea Mountains that suppressed precipitation over the Central Pangean Mountains and shifted the ITCZ poleward, like the monsoonal circulation (e.g. Heavens et al., 2015). This model considers the prevailing winds would have been laden with moisture evaporated from Palaeo-Tethys and wind from the east during equatorial glaciations, which is not in agreement with the wind direction measured in Paradox Basin (this study and e.g. Loope, 1984; Soreghan *et al.*, 2002b; Mountney, 2006). In western equatorial Pangea and in the Paradox Basin, Soreghan *et al.* (2008) considered loess-paleosols to record sub-100 kyr fluctuations between the drier, dustier glacial periods, and the wetter interglacial intervals of the late Palaeozoic (Soreghan et al., 2014a, b). The paleowind directions in this region are oriented to the south-southwest, reflective of a megamonsoonal circulation formed during the assembly of the Pangea (e.g. Soreghan *et al.*, 2002b). These authors consider a glacial and thus primarily mechanical weathering as origin of the silt. However, the paleowind measurements in aeolian dunes in our study area have the same orientation of those measured

by Soreghan *et al.* (2002b) and consequently, this loess, if time equivalent to the aeolian dunes in the coastal domain, could correspond to aeolian sand reworked from the coastal region. Such an origin would therefore reflect monsoonal conditions fostering strong winds, seasonality, and consequent silt mobilization, instead of the existence of uplands and cold-weathering processes at low latitude (e.g. Soreghan *et al.*, 2008). Moreover, Griffis et al. (2022) also suggest a non-glacial origin for the silt. Overall, at this period of the Earth history, i.e. Late Pennsylvanian to early Permian, in the western Pangean domain, a large quantity of aeolian dust is available and preserved, whereas in the eastern Pangean domain, coal, lacustrine deposits with Gilbert-type deltas and volcanic ashes are recorded (Schneider *et al.*, 2006; Ducassou *et al.,* 2019; Mercuzot *et al.*, 2021). Consequently, aeolian deposits are equivalent to the end of the glacial phase, and the glacial phase, with peat/coal development in the terrestrial domain, could be equivalent to fluvial and mouth-bar deposits in the coastal domain located just above well-developed paleosols, at the beginning of the glacial phase, as described in American Midcontinent during Late Pennsylvanian (e.g. Cecil *et al.*, 2014).

7.3. Provenance and tectonics

The Paradox Basin display bimodal detrital-zircon age indicating fluvial sediment derived from local basement of Uncompahgre Highland but the source of Neoproterozoic grains in marine and aeolian sandstones along the marine shoreline remains uncertain (e.g. Lawton *et al.*, 2021). However, for the White Rim Sandstone, Lawton *et al.* (2015) considered that sediment was transported via transcontinental rivers to the western marine margin of Laurentian Pangea from the Appalachian region, and abundant sediment was blown southeastward from littoral sources incrementally exposed during Kungurian sea-level drawdown. Rapid transport of voluminous aeolian sediment overwhelmed sediment derived from local Uncompahgre sources and resulted in observed compositional changes in aeolian relative to fluvial sediment.

In the northeastern part of the Paradox Basin, the sedimentation of the Undivided Cutler Gp is controlled by high subsidence rate with syn-sedimentary fault (e.g. Wengerd & Matheny, 1958; Condon, 1997; Venus *et al.*, 2015; Lawton et al., 2015). However, in our studied area the subsidence rate is considered as relatively constant as proved by the tabular correlation. If the first order control on the depositional environment, i.e. genetic unit and minor cycles, is glacio-eustasy and thus is linked to the climate condition of the equatorial domain, the general evolution of the series, i.e. M1 and M2 cycles, could reflect another control (Fig. 17). Indeed, the first major progradational-retrogradational pattern, M1, seems to be controlled by large-scale sea-level variations, whereas the progradational phase of the M2 cycle seems to be controlled by local sediment supply variation (Fig. 17). In fact, the upper part of the succession is marked by an increase in fluvial sediment supply within the same climate context (indicated by the same association of calcretes, paleosol and aeolian deposits southward), which is therefore probably linked with the syn-sedimentary movements recorded in the northeast part of the study area observed at that time in the Undivided Cutler Gp (Venus *et al.*, 2015). However, Moore *et al.* (2008) suggest that movement along the subsurface Uncompahgre fault had ceased by then. Moreover, according to Soreghan *et al.* (2009, 2014a) and Keiser *et al.* (2015), the Undivided Cutler Gp is described as a proglacial to periglacial lacustrine system in proximity of marine and paralic facies, which implies cold temperature at low elevations in the Uncompahgre Highland. If this local glaciation were to have taken place it would have required anomalously cold conditions in an equatorial domain, which poses the question of the contemporaneity of this formation with the other formations in the basin.

8. Conclusion

Interactions between aeolian, fluvial and marine environments within the entire Permian succession of the Canyonlands area in Utah have been demonstrated from a detailed facies analysis and high-resolution sequence stratigraphic correlation. Vertical evolution of depositional environments shows, at Late Pennsylvanian - early Permian transition, mixed-shoreface, mouth-bar and braided-rivers deposits with preservation of large trees. This depositional environment evolves vertically with an increasing preservation of aeolian dunes and decreasing fluvial influences with preservation of root traces. The upper part records an increase in fluvial sediment supply in the north, which caused a decrease of aeolian preservation, always within a marine coastal environment. The longshore bar facies become less developed and the mouth-bar deposits dominate the marine sedimentation.

The detailed exposures of high-frequency cycles of erg construction and marine flooding under some fluvial influence in the Permian of Utah provide a valuable analogue for other records, especially within subsurface data. Moreover, in the palaeogeographic and LPIA contexts, a scenario is proposed to explain the stratigraphic cycles, and the variation of depositional environments and vegetation preservation observed in the Late Pennsylvanian - early Permian, considering sea-level and sediment supply variations within glacial-interglacial phases in the equatorial Pangea. Two types of fluvial deposits are recognized. The first one, above the longshore dunes, appears at the minimum of sea-level fall or beginning of the lowstands, during the glacial phase, and is in a progradational setting, overlain by aeolian dune fields. The second one, very rarely preserved, is above the aeolian dune fields and occurs during the acceleration of the transgression, at the beginning of the interglacial stage. Aeolian environments occur at the end of lowstands, during the beginning of sea-level rise, at the transition to the interglacial stage. Two stages of paleosol preservation are observed. One occurs during initiation of ice build-up, i.e. during sea-level fall. The second occurs during transgression and the beginning of the interglacial stage, which allows aeolian dune preservation. As a consequence, in this equatorial coastal domain, the aeolian deposits reflect a period of a reduction of vegetation that was accompanied by greater erosion. This occurred during the beginning phases of sea-level rise and is probably also related to the onset of a more extensive seasonal migration of the Intertropical Convergence Zone with higher wind velocities.

Acknowledgments

This work was part of Marie Olivier's thesis (supervised by S. Bourquin and co-supervised by G. Desaubliaux) and is funded by GDF-Suez/CNRS research collaboration contract (LS 74898). We particularly thank William A. DiMichele for the discussions, for the critical rereading of this text, and thus for the help to improve this manuscript. We thank X. Le Coz (Geosciences Rennes) for the preparation of thin sections. We also thank two anonymous reviewers for their constructive comments that improved this manuscript.

References

945 Allen, J.R.L., Banks, N.L., 1972. An Interpretation and Analysis of Recumbent Folded
946 Deformed cross Bedding. Sedimentology 19, 257-283.

947 Baars, D. L., 1962. Permian system of Colorado Plateau. AAPG Bull. 46, 2, 149-218.

948 Baars, D. L., 1975. The Permian System of Canyonlands country. In: Fassett, J.E. (Ed),
949 Canyonlands Country. 8th Field Conference, Four Corners Geol. Soc. Guidebook, pp. 123-
950 128.

951 Baars, D.L., 1979. The Permian System. In: Baars, D.L. (Ed), Permianland. 9th Field
952 Conference, A Field Symposium, Four Corners Geol. Soc. Guidebook, pp. 1-6.

953 Baars, D.L., 1987. Paleozoic rocks of Canyonlands country. In: Campbell, J.A. (Ed), Geology
954 of Cataract Canyon and Vicinity. 10th Field Conference, A Field Symposium, Four
955 Corners Geol. Soc. Guidebook, pp. 11-16.

956 Baars, D. L., Molenaar, C.M., 1971. Geology of Canyonlands and Cataract Canyon. 6th Field
957 Four Corners Geol. Soc. Conference, Durango, Colorado, USA, 99.

958 Baker, A.A., Reeside Jr., J.B., 1929. Correlation of the Permian of southern Utah, northern
959 Arizona, northwestern New Mexico, and southwestern Colorado. AAPG Bull. 13, 1413-
960 1448.

961 Blakey, R.C., 1979. Lower Permian stratigraphy of the southern Colorado Plateau. In: Baars,
962 D.L. (Ed), Permianland. 9th Field Conference Four Corners Geological Society Guidebook,
963 pp. 115-129.

964 Blakey, R.C., 1980. Pennsylvanian and Early Permian paleogeography, southern Colorado
965 Plateau and vicinity. In: Fouch, T.D., Magathan, E.R., (Eds), Paleozoic Paleogeography of
966 West-Central United States. SEPM, Rocky Mt. Section, pp. 239-257.

967 Blakey, R.C., 1988. Basin tectonics and erg response: Sed. Geol. 56, pp. 127-151.

968 Blakey, R.C., 1996. Permian deposits, sequences, and sequence boundaries, Colorado Plateau.
969 In: Longman, M.W., Sonnenfeld, M.D., (Eds) Paleozoic Systems of the Rocky Mountain
970 Region. Rocky Mt. Sect. SEPM, Rocky Mountain section, pp. 405-426.

971 Blakey, R.C., 2008. Pennsylvanian–Jurassic sedimentary basins of the Colorado Plateau and
972 southern RockyMountains. In: Miall, A.D. (Ed.), Sedimentary Basins of the United States
973 and Canada. Elsevier, Amsterdam, pp. 245–296

974 Blakey, R.C., Havholm, K.G. Jones, L.S., 1996. Stratigraphic analysis of eolian interactions
975 with marine and fluvial deposits, Middle Jurassic Page Sandstone and Carmel Formation,
976 Colorado Plateau, USA. J. Sed. Res. B, 66, 324-342.

977 Blakey, R.C., Peterson, F., Kocurek, G., 1988. Late Paleozoic and Mesozoic eolian deposits
978 of the Western Interior of the United States. Sed. Geol. 56, 3-125.

979 Blanchard, S., Fielding, C.R., Frank, T.D., Barrick, J.E., 2016. Sequence stratigraphic
980 framework for mixed aeolian, peritidal and marine environments: Insights from the
981 Pennsylvanian subtropical record of Western Pangaea. Sedimentology 63, 7, 1929-1970.
982 doi: 10.1111/sed.12285.

983 Bourquin, S., Eschard, R., Hamouche, B., 2010. High-resolution sequence stratigraphy of
984 Upper Triassic succession (Carnian Rhaetian) of the Zarzaitine outcrops (Algeria): a model
985 of fluvio-lacustrine deposits. J. Afr. Earth Sci. 58, 365-386

986 Bourquin, S., Guillocheau, F., Péron, S., 2009. Braided rivers within an arid alluvial plain
987 (example from the Lower Triassic, western German Basin): recognition criteria and
988 expression of stratigraphic cycles. Sedimentology 56, 2235-2264.

989 Bourquin, S., Rigollet, C., Bourges, P., 1998. High-resolution sequence stratigraphy of an
990 alluvial fan-fan delta environment: stratigraphic and geodynamic implication. An example
991 from the Keuper Chaunoy Sandstones, Paris Basin. Sed. Geol. 121, 207-237.
992 Buatois L., Mángano, M.G., 2011. Ichnology: Organism-Substrate Interactions in Space and
993 Time, Cambridge Univ. Press.
994 Brookfield, M.E., Silvestro, S., 2010. Eolian systems. In: James, N.J., Dalrymple, R.W. (Eds),
995 Facies Models 4. GEOtext 6, Geol. Association Canada, pp. 139-166.

996 Cain, S.A., Mountney, N. P., 2009. Spatial and temporal evolution of a terminal fluvial fan
997 system: the Permian Organ Rock Formation, South-east Utah, USA. Sedimentology 56, 6,
998 1774-1800.

999 Cain, S.A., Mountney, N. P., 2011. Downstream Changes and Associated Fluvial-Eolian
1000 Interactions in an Ancient Terminal Fluvial System: The Permian Organ Rock Formation,
1001 Se Utah, USA. In:, S., Leleu S., North C.P., From River to Rock Record: The preservation
1002 of fluvial sediments and their subsequent interpretation. SEPM Spec. Publ. 97, 165-187.

1003 Campbell, J.A., 1980. Lower Permian depositional systems and Wolfcampian
1004 paleogeography, Uncompahgre basin, eastern Utah and southwestern Colorado. In: Fouch,
1005 T.D., Magathan, E.R. (Eds), Paleozoic Paleogeography of West-Central United States.
1006 SEPM, Rocky Mt. Section, pp. 327-340.

1007 Carr-Crabaugh, M., Dunn, T. 1996. Reservoir Heterogeneity as a Function of Accumulation
1008 and Preservation Dynamics, Tensleep Sandstone, Bighorn and Wind River Basins,
1009 Wyoming. SEPM, Rocky Mt. Section, pp. 305-320.

1010 Carr-Crabaugh, M., Kocurek, G., 1998. Continental sequence stratigraphy of a wet eolian
1011 system: A key to relative sea-level change. In: Stanley, K.W., McCabe, P.J. (Eds), Relative
1012 Role of Eustasy, Climate, and Tectonics in Continental Rocks. SEPM Spec. Publ. 59, pp.
1013 213-228.

1014 Catuneanu, O., Abreu, V., Bhattacharya, J.P., Blum, M.D., Dalrymple, R.W., Eriksson, P.G.,
1015 Fielding, C.R., Fisher, W.L., Galloway, W.E., Gibling, M.R., Giles, K.A., Holbrook, J.M.,
1016 Jordan, R., Kendall, C.G.S.C., Macurda, B., Martinsen, O.J., Miall, A.D., Neal, J.E.,
1017 Nummedal, D., Pomar, L., Posamentier, H.W., Pratt, B.R., Sarg, J.F., Shanley, K.W.,
1018 Steel, R.J., Strasser, A., Tucker, M.E., and Winker, C., 2009. Towards the standardization
1019 of sequence stratigraphy. Earth Sci. Rev. 92, 1-33.
1020 Cecil, C.B., Dulong, F.T., West, R.R., Stamm, R., Wardlaw, B., Edgar, N.T., 2003. Climate
1021 controls on the stratigraphy of a Middle Pennsylvanian Cyclothem in North America.
1022 SEPM Spec. Publ. 77, 151-180.

1023 Cecil, C.B., DiMichele, W.A., Elrick, S.D., 2014. Middle and Late Pennsylvanian
1024 cyclothems, American Midcontinent: Ice-age environmental changes and terrestrial biotic
1025 dynamics. C. R. Geoscience 346, 7-8, 159-168.

1026 Chan, M. A., Kocurek, G., 1988. Complexities in eolian and marine interactions: processes
1027 and eustatic controls on erg development. Sed. Geol. 56, 1-4, 283-300.

1028 Chan, M.A., 1989. Erg margin of the Permian White Rim Sandstone, southeastern Utah.
1029 Sedimentology 36, 235-251.

1030 Clemmensen, L.B., Abrahamsen, K., 1983. Aeolian stratification and facies association in
1031 desert sediments, Arran basin (Permian), Scotland. Sedimentology 30, 311-339.
1032 Clemmensen, L.B., Olsen, H., Blakey, R.C., 1989. Erg-margin deposits in the Lower Jurassic
1033 Moenave Formation and Wingate Sandstone, southern Utah. Geol. Soc. Am. Bull. 101,
1034 759-773.

1035 Clemmensen, L.B., Tirsgaard, H., 1990. Sand-drift surfaces: a neglected type of bounding
1036 surface. Geology 18, 11, 1142-1145.

1037 Colson, J., Cojan, I., 1996. Groundwater dolocretes in a lake-marginal environment: an
1038 alternative model for dolocrete formation in continental settings (Danian of the Provence
1039 Basin, France). Sedimentology 43, 1, 175–188. https://doi.org/10.1111/j.1365-
1040 3091.1996.tb01466.x

1041 Condon, S.M., 1997. Geology of the Pennsylvanian and Permian Cutler Group and Permian
1042 Kaibab Limestone in the Paradox basin, southeastern Utah and southwestern Colorado. US
1043 Geol. Survey Bull. 2000, 46.

1044 Cross, T.A., 1988. Controls on coal distribution in transgressive-regressive cycles, Upper
1045 Cretaceous, Western Interior, USA. In: Wilgus, C.K., Hastings, B.S., Kendall, C.G.St.C.,
1046 Posamentier, H.W., Ross, C.A., Van Wagoner, J.C. (Eds), Sea-level changes: an integrated
1047 approach. SEPM Spec. Publ. 42, pp. 371-380.

1048 Cross, T.A,. Baker, M.R., Chapin, M.A., Clark, M.S., Gardner, M.S., Hanson, M.A.,
1049 Lessenger, L.D., Little, L.D., Mc Donough, K.-J., Sonnenfield, M.D., Valesk, M.R.,
1050 Williams, M.R., Witter, D.N., 1993. Applications of high-resolution sequence stratigraphy
1051 to reservoir analysis. In: Eschard, R. and Doligez, B. (Eds), Subsurface Reservoir
1052 Characterisation from Outcrop Observations. Technips Editions, pp. 11-33.
1053 Currie, B.S., 1997. Sequence stratigraphy of nonmarine Jurassic-Cretaceous rocks, central
1054 Cordilleran foreland-basin system. Geol. Soc. Am. Bull. 109, 1206-1222.

1055 Dalrymple, R.W., 2010. Tidal Depositional Systems. In: James, N.J. and Dalrymple, R.W.
1056 (Eds), Facies Models 4. GEOtext 6, Geol. Association Canada, pp. 201-232.

1057 DiMichele, W.A., 2014. Wetland-dryland vegetational dynamics in the Pennsylvanian ice age
1058 tropics. Int. J. Plant Sci. 175(2):123–164. DOI: 10.1086/675235

1059 DiMichele, W.A., Chaney, D.S., Nelson, W.J. Lucas, S.G., Looy, C.V., Quick, K., Wang J.
1060 2007. A low diversity, seasonal tropical landscape dominated by conifers and peltasperms:
1061 Early Permian Abo Formation, New Mexico. Rev. Palaeobot. Palynol. 145, 249-273.

DiMichele, W.A., Cecil, C.B., Chaney, D.S., Elrick, S.D., and Nelson, W.J., 2014, Fossil floras from the Pennsylvanian-Permian Cutler Group of southeastern Utah. In: MacLean, J.S., Biek, R.F., Huntoon, J.E. (Eds), Geology of Utah's Far South: Utah Geol. Association Publ. 43, p. 491-504

Doe, T.W., Dott, J.R., 1980. Genetic significance of deformed cross bedding – with examples from the Navajo and Weber sandstones of Utah. J. Sed. Petrol. 50, 3, 0793 – 0812.

Dubiel, R.F., Huntoon, J.E., Condon, S.M., Stanesco, J.D., 1996. Permian deposystems, palaeogeography, and palaeoclimate of the Paradox Basin and vicinity. In: Longman M.W. and Sonnenfeld, M.D. (Eds), Palaeozoic Systems of the Rocky Mountain Region. SEPM, Rocky Mt. Section, pp. 427-444.

Ducassou, C., Mercuzot, M., Bourquin, S., Rossignol, C., Beccaletto, L., Pierson-Wickmann, A.C., Pellenard, P., Poujol, M., Hue, C., 2019. Sedimentology and U-Pb dating of Carboniferous to Permian continental series of the northern Massif Central (France): local palaeogeographic evolution and larger scale correlations. Palaeogeogr., Palaeocl., Palaeoec. 533, https://doi.org/10.1016/j.palaeo.2019.06.001

Falcon-Lang, H.J., Jud, N.A., Nelson, W.J., DiMichele, W.A., Chaney, D.S., Lucas, S.G., 2011. Pennsylvanian coniferopsid forests in sabkha facies reveal the nature of seasonal tropical biome. Geology 39, 371–374.

Falcon-Lang, H.J., Lucas, S.G., Kerp, H., Krainer, K., Montañez, I.P., Vachard, D., Chaney, D.S., Contreras, D.L., Kurzawe, F., DiMichele, W.A., Looy, C.V., 2015. Early Permian (Asselian) vegetation from a seasonally dry coast in western equatorial Pangea: Paleoecology and evolutionary significance. Palaeogeogr., Palaeocl., Palaeoec. 433, 158-173

Falcon-Lang, H.W., Kurzawe, F., Lucas, S.G., 2016. A Late Pennsylvanian coniferopsid forest in growth position, near Socorro, New Mexico, USA: Tree systematics and palaeoclimatic significance. Rev. Palaeobot. Palynol. 225, 67-83.

Fielding, C.R., Frank, T.D., Isbell, J.L., 2008. The late Paleozoic ice age a review of current understanding and synthesis of global climate patterns. In: Fielding, C.R., Frank, T.D., Isbell, J.L. (Eds), Resolving the Late Paleozoic Ice Age in Time and Space. Geol. Soc. Am. Spec. Pap. 441, pp. 343-354.

Fryberger S.G., Al-Sari, A.M., Clisham, T.J., Rizvi, S.A.R., Al-Hinai, K.G., 1984. Wind sedimentation in the Jafurah sand sea, Saudi Arabia. Sedimentology 31, 413-31.

Fryberger, S.G., 1993. A review of aeolian bounding surfaces, with examples from the Permian Minnelusa Formation, USA. In: North, C.P., Prosser, D.J (Eds), Characterisation of Fluvial and Aeolian Reservoirs. Geol. Soc. London Spec. Publ. 73, pp. 167-19.

Gerard, J.R.F, Bromley, F.G., 2008. Ichnofabrics in clastic sediments: applications to sedimentological core studies, a practical guide. Madrid: R.F. Gerard, 97.

Gregory, H.E., 1938. The San Juan country, a geographic and geologic reconnaissance of southeastern Utah, US Geol. Survey Prof. Pap. 188, 123.

Griffis, N., Mundil, R., Montanez, I., Le Heron, D., Dietrich, P. Iannuzzi, R, 2022. A Carboniferous Apex for the late Paleozoic Icehouse. Geol. Soc. London Spec. Publ., doi.org/10.1144/SP535-2022-256

Gross E.C., Carr M, Jobe Z.R. 2022. Three-dimensional bounding surface architecture and lateral facies heterogeneity of a wet aeolian system: Entrada Sandstone, Utah. Sedimentology 70**, 145–178,** doi: 10.1111/sed.13035

Hasiotis, S.T., Bourke, M.C., 2006. Continental trace fossils and museum exhibits: displaying burrows as organism behaviour frozen in time. Geol. Curator 8, 5, 211-226.

Hasiotis, S.T., Kraus, M.J., Demko, T., 2007. Climatic Controls on Continental Trace Fossils. In: Miller, W. (Ed), Trace Fossils: Concepts, Problems, Prospects. Elsevier 1st Ed, pp. 172-195.

Havholm, K.G., Blakey, R.C., Capps, M., Jones, L.S., King, D.D., Kocurek, G., 1993. Aeolian genetic stratigraphy: an example from the Middle Jurassic Page Sandstone, Colorado Plateau. In: Lancaster, N. (Ed), Aeolian Sediments: Ancient and Modern. Blackwell Sci. Publ. Oxford 165, pp. 87-107.

Helland-Hansen, W., Martinsen, O.J., 1996. Shoreline trajectories and sequences: description of variable depositional-dip scenarios J. Sed. Res. 66, 670-688.

Heavens N.G., Mahowald N.M., Soreghan G.S., Soreghan M.J., Shields C.A., 2015. A model-based evaluation of tropical climate in Pangea during the late Paleozoic icehouse. Palaeogeogr., Palaeocl., Palaeoec. 425, 109-127.

Hême de Lacotte V.J.P., Mountney N.P. 2022. A classification scheme for sedimentary architectures arising from aeolian-fluvial system interactions: Permian examples from southeast Utah, USA. Aeol. Res. 58, doi.org/10.1016/j.aeolia.2022.100815.

Hinds, D.J., Aliyeda, E., Allen, M.B., Davies, C.E., Kroonenberg, S.B., Simmons, M.D., Vincent, S.J., 2004. Sedimentation in a discharge dominated fluvial-lacustrine system: the Neogene Productive Series of the South Caspian Basin, Azerbaijan. Mar. Petrol. Geol.21, 613-638.

Hunter, R.E., 1977. Basic types of stratification in small eolian dunes Sedimentology 24, 361-387.

Huntoon, J.E., Chan, M.A., 1987. Marine origin of paleotopographic relief on eolian White Rim Sandstone (Permian), Elaterite basin, Utah. AAPG Bull. 71, 1035–1045. https://doi.org/10.1306/703C7DEF-1707-11D7-8645000102C1865D.

Jervey, M.T., 1988. Quantitative geological modeling of siliciclastic rock sequences and their seismic. In: Wilgus, C.K., Hastings, B.S., Kendall, C.G.St.C., Posamentier, H.W., Ross, C.A., Van Wagoner, J.C. (Eds), Sea-level changes: an integrated approach. SEPM Spec. Publ. 42, pp. 47-70.

Jordan, O.D., Mountney, N.P., 2010. Styles of interaction between aeolian, fluvial and shallow marine environments in the Pennsylvanian to Permian lower Cutler beds, south-east Utah, USA. Sedimentology 57, 5, 1357-1385.

1140 Jordan, O.D., Mountney, N.P., 2012. Sequence stratigraphic evolution and cyclicity of an
1141 ancient coastal desert system: the Pennsylvanian–Permian lower Cutler beds, Paradox
1142 Basin, Utah, USA. J. Sed. Res. 82, 10, 755-780.

1143 Kamola, D.L., Chan, M.A., 1988. Coastal dune facies, Permian Cutler Formation (White Rim
1144 Sandstone), Capitol Reef National Park area, southern Utah. Sed. Geol. 56, 341–356.
1145 https://doi.org/10.1016/0037-0738(88)90060-7.

1146 Keiser, L., Soreghan, G.S., Kowalewski, M., 2015. Use of Quartz Microtextural Analysis To
1147 Assess Possible Proglacial Deposition For the Pennsylvanian–Permian Cutler Formation
1148 (Colorado, USA). J. Sed. Res. 85, 11,1310

1149 Kocurek, G., Fielder, G., 1982. Adhesion structures. J. Sed. Petrol.,52, 4, 1129-1241.

1150 Kocurek, G., 1988. First-order and super bounding surfaces in eolian sequences-bounding
1151 surfaces revisited. Sed. Geol. 56, 1-4, 193-206.

1152 Kocurek, G., Nielson, J., 1986. Conditions favourable for the formation of warm-climate
1153 aeolian sand sheets. Sedimentology 33, 795-816.
1154 Kocurek, G., Havholm, K.G., 1993. Eolian sequence stratigraphy: A conceptual framework.
1155 In: Weimer, P., Posamentier, H.W. (Eds), Siliciclastic Sequence Stratigraphy: Recent
1156 Developments and Applications. AAPG Mem. 58, pp. 393-410.

1157 Kocurek, G., Fielder, G., 1982. Adhesion structures. J. Sed. Petrol. 52, 4, 1229–1241

1158 Kunkel, R.P., 1958. Permian stratigraphy of the Paradox basin. In: Sanborn, A.F., (Ed),
1159 Guidebook to the Geology of the Paradox Basin Intermountain. Association Petrol. Geol.,
1160 Salt Lake City, Utah, pp. 163-168.

1161 Langford, R.P., Chan, M.A., 1989. Fluvial-aeolian interactions: Part II, ancient systems.
1162 Sedimentology 36, 1037-1051.
1163 Langford, R.P., Chan, M.A., 1988. Flood surfaces and deflation surfaces within the Cutler
1164 Formation and Cedar Mesa Sandstone (Permian), southeastern Utah. Geol. Soc. Am. Bull.
1165 100, 1541-1549.

1166 Langford, R.P., Chan, M.A., 1993. Downwind Changes within an Ancient Dune Sea, Permian
1167 Cedar Mesa Sandstone, Southeast Utah. In: Pye, K., Lancaster, N. (Eds), Aeolian
1168 sediments ancient and modern. IAS Spec. Publ. 16., pp. 109-126.
1169 Leeder, M.R., Stewart, M.D., 1996. Fluvial incision and sequence stratigraphy: alluvial
1170 responses to relative sea-level fall and their detection in the geological record. Geol. Soc.
1171 London Spec. Publ. 103, 25–39.

1172 Legarreta, L., Uliana, M.A., Larotonda, C.A., Meconi, G.R., 1993. Approaches to nonmarine
1173 sequence stratigraphy-theorical models and examples from Argentine basins. In: Eschard,
1174 R., Doligez, G. (Eds), Subsurface reservoirs characterisation from outcrop observations. 7th
1175 IFP Exploration and Production Research Conference, Technips Editions, pp. 125-143.
1176 Loope, D.B., 1981. Deposition, deflation, and diagenesis of upper Paleozoic eolian sediments,
1177 Canyonlands National Park. Utah Ph.D. diss. Univ. Wyoming, 170.

1178 Loope, D.B., 1984. Eolian origin for upper Paleozoic Sandstones, southeastern Utah. J. Sed.
1179 Petrol. 54, 563-580.

1180 Loope, D.B., 1985. Episodic deposition and preservation of Aeolian sands: a late Paleozoic
1181 example from southeastern Utah. Geology 13, 73-76.

1182 Lowe, D.R., 1982. Sediment gravity flows: II. Depositional models with special reference to
1183 the deposits of high-density turbidity currents. J. Sed. Petrol. 52, 1, 279-297.
1184 Lawton, T.F., Buller, C.D., and Parr, T.R., 2015. Provenance of a Permian erg on the western
1185 margin of Pangea: Depositional system of the Kungurian (late Leonardian) Castle Valley
1186 and White Rim sandstones and subjacent Cutler Group, Paradox Basin, Utah, USA:
1187 Geosphere 11, 5, p. 1475–1506, doi:10.1130/GES01174.1

1188 Lawton, T.F., Blakey, R.C., Stockli, D.F., Liu, L. 2021. Late Paleozoic (Late Mississippian–
1189 Middle Permian) sediment provenance and dispersal in western equatorial Pangea.
1190 Palaeogeogr., Palaeocl., Palaeoec. 572, 110386, ISSN 0031-0182,
1191 https://doi.org/10.1016/j.palaeo.2021.110386.

1192 Lucas, S.G., Henderson, C.M., 2021. New age data for Permian strata on the Mogollon Rim,
1193 central Arizona, USA. Permophiles, 71, 18-21

1194 Mack, G.H., 1977. Depositional environments of the Cutler–Cedar Mesa facies transition
1195 (Permian) near Moab, Utah Mt. Geol. 14, 53-68.

1196 Mack, G.H., 1978. The survivability of labile light-mineral grains in fluvial, eolian, and
1197 littoral marine environments: the Permian Cutler and Cedar Mesa Formations, Moab, Utah.
1198 Sedimentology 25, 587-604.

1199 Mack, G.H., 1979. Littoral marine depositional model for the Cedar Mesa Sandstone
1200 (Permian), Canyonlands National Park, Utah Permianland. 9th Field Conference, Four
1201 Corners. Geol. Soc. Guidebook, 33-37.

1202 Mack, G.H., Rasmussen, K.A., 1984. Alluvial fan sedimentation of the Cutler Formation
1203 (Permo-Pennsylvanian) near Gateway, Colorado. Geol. Soc. Am. Bull.95, 109-116.

1204 Mamay, S.H., Chaney, D.S., DiMichele, W.A., 2009. Comia, a seed plant possibly of
1205 peltaspermous affinity: a brief review of the genus and description of two new species
1206 from the Early Permian (Artinskian) of Texas, C. greggii sp. nov. and C. craddockii sp.
1207 nov. Int. J. Plant Sci.170, 267–282.

1208 Marshall, J.D., 2000. Sedimentology of a Devonian fault-bounded braidplain and lacustrine
1209 fill in the lower part of the Skrinkle Sandstones, Dyfed, Wales. Sedimentology 47, 325-
1210 342.

1211 Mercuzot, M., Bourquin, S., Beccaletto, L., Ducassou, C., Rubi, R., Pellenard, P., 2021.
1212 Palaeoenvironmental reconstitutions at the Carboniferous-Permian transition south of the
1213 Paris Basin, France: implications on the stratigraphic evolution and basin geometry. Int. J.
1214 Earth Sci.1-25, https://doi.org/10.1007/s00531-020-01940-7

1215 Miall, A.D., 1978. Lithofacies types and vertical profile models in braided river deposits: a
1216 summary. In: Miall, A.D. (Ed), Fluvial sedimentology. Canadian Soc. Petrol. Geol. 5, pp.
1217 597-604.
1218 Miall, A.D., 1996. The geology of fluvial deposits. Springer-Verlag, 582.

1219 Mitchum Jr., R.M., Van Wagoner, J.C., 1991. High-frequency sequences and their stacking
1220 patterns: sequence-stratigraphic evidence of high-frequency eustatic cycles. Sed. Geol. 70,
1221 131-160.
1222 Montañez, I.P., McElwain, J.C., Poulsen, C. J., White, J.D., DiMichele, W.A., Wilson, J.P.,
1223 Griggs, G., Hren, M.T., 2016. Climate, pCO2 and terrestrial carbon cycle linkages during
1224 late Palaeozoic glacial-interglacial cycles. Nature Geosci. 9, 824–828,

1225 Moore, K.D., Soreghan, G.S., Sweet D.E., 2008. Stratigraphy and structural relations in the
1226 proximal Cutler Formation of the Paradox Basin: implication for Timing of movement on
1227 the Uncompahgre front. Mt Geol. 45, 2, 49-68

1228 Mountney, N.P., 2006. Periodic accumulation and destruction of aeolian erg sequences in the
1229 Permian Cedar Mesa Sandstone, White Canyon, southern Utah, USA. Sedimentology 53,
1230 789–823.

1231 Mountney, N. P., 2012. A stratigraphic model to account for complexity in aeolian dune and
1232 interdune successions. Sedimentology 59, 3, 964-989.
1233 Mountney, N.P., Jagger, A., 2004. Stratigraphic evolution of an aeolian erg margin system:
1234 the Permian Cedar Mesa Sandstone, SE Utah, USA. Sedimentology 51, 713-743.

1235 Mulder, T., Alexander, J., 2001. The physical character of subaqueous sedimentary density
1236 flows and their deposits. Sedimentology 48, 259-299.
1237 Olariu, C, Steel, R.J., Dalrymple, R.W., Gingras, M.K., 2012. Tidal dunes versus tidal bars:
1238 The sedimentological and architectural characteristics of compound dunes in a tidal
1239 seaway, the lower Baronia Sandstone (Lower Eocene), Ager Basin, Spain. Sed. Geol. 279,
1240 134-155.
1241 Olsen, T., 1995. Sequence stratigraphy, alluvial architecture and potential reservoir
1242 heterogeneities of fluvial deposits: evidence from outcrop studies in Price Canyon, Utah
1243 (Upper Cretaceous and Lower Tertiary). In: Steel, R.J. (Ed), Sequence Stratigraphy on the
1244 Northwest European Margin. Elsevier, 5, NPF Spec. Publ., pp. 75-96.
1245 Olszewski, T.D., Patzkowsky, M.E., 2003. From cyclothems to sequences: the record of
1246 eustasy and climate on an icehouse epeiric platform (Pennsylvanian–Permian, North
1247 American Midcontinent). J. Sed. Res. 73, 15–30

1248 Orgill, J.R., 1971. The Permian-Triassic unconformity and its relationship to the Moenkopi,
1249 Kaibab, and White Rim Formations in and near San Rafael Swell, Utah. Brigham Young
1250 Univ. Geol. Studies 18, 3, 131-179.

1251 Peterson, F., 1988. Pennsylvanian to Jurassic eolian transportation systems in the western
1252 United States. Sed. Geol. 56, 207-260.

1253 Pettigrew, R.P., Priddy, C. Clarke, S.M., Warke, M.R., Stüeken, E.E., Claire, M.W., 2021.
1254 Sedimentology and isotope geochemistry of transitional evaporitic environments within
1255 arid continental settings: From erg to saline lakes. Sedimentology 68, 3, 907-942.

1256 Plint, A.G., 2010. Wave and Storm-Dominated Shoreline and Shallow-Marine Systems. In:
1257 James, N.J., Dalrymple, R.W. (Eds), Facies Models 4. GEOtext 6, Geol. Association
1258 Canada, pp. 167-200.

1259 Pollard, J.E., Steel, R.J., Undersrid, E., 1982. Facies sequences and trace fossils in
1260 lacustrine/fan delta deposits, Hornelen Basin (M. Devonian), Western Norway. Sed. Geol.
1261 32, 63-87.

1262 Posamentier, H.W., Vail, P.R., 1988. Eustatic controls on clastic deposition II. Sequence and
1263 systems tract models. In: Wilgus, C.K., Hastings, B.S., Kendall, C.G.St.C., Posamentier,
1264 H.W., Ross, C.A., Van Wagoner, J.C. (Eds), Sea-level changes: an integrated approach.
1265 SEPM Spec. Publ. 42, pp. 125-154.
1266 Posamentier, H.W. Jervey, M.T., Vail, P.R., 1988. Eustatic controls on clastic deposition I.
1267 Conceptual framework. In: Wilgus, C.K., Hastings, B.S., Kendall, C.G.St.C., Posamentier,
1268 H.W., Ross, C.A., Van Wagoner, J.C. (Eds), Sea-level changes: an integrated approach.
1269 SEPM Spec. Publ. 42, pp. 109-124.
1270 Postma, G., 1990. Depositional architecture and facies of river and fan deltas: a synthesis. In:
1271 Colella, A., David, B.P. (Eds), Coarse-grained Deltas. International Association of
1272 Sedimentologists Spec. Publ. 10, pp. 13-28.
1273 Rankey, E.C., 1997. Relations between relative changes in sea level and climate shifts:
1274 Pennsylvanian–Permian mixed carbonate-siliciclastic strata, western United States. Geol.
1275 Soc. Am. Bull. 109, 1089–1100
1276 Retallack, G.J., 1988. Field recognition of paleosols. In: Reinhardt, J., Sigleo, W.R. (Eds),
1277 Paleosols and Weathering Through Geologic Time: Principles and Applications. Geol.
1278 Soc. Am. Spec. Pap. 21, pp. 1-20.
1279 Rygel, M.C., Fielding, C.R., Frank, T.D., Birgenheier, L.P., 2008. The magnitude of late
1280 Palaeozoic glacioeustatic fluctuations: a synthesis. J. Sed. Res. 78, 500-511.

1281 Sanderson, G.A., Verville, G.J., 1990. Fusulinid Zonation of the General Petroleum No. 4 5 5
1282 4 Core, Emery County, Utah1. Mt Geol. 27, 4, 131-136.

1283 Schneider, J.W., Körner, F., Roscher, M., Kroner, U., 2006. Permian climate development in
1284 the northern peri-Tethys area - The Lodève basin, French Massif Central, compared in a
1285 European and global context. Palaeogeogr., Palaeocl., Palaeoec. 240, 161-183.
1286 https://doi.org/10.1016/j.palaeo.2006.03.057

1287 Schultz, A.W., 1984. Subaerial debris-flow deposition in the Upper Paleozoic Cutler
1288 Formation, western Colorado. J. Sed. Petrol.,54, 759-772.

1289 Shanley, K.W., McCabe, P.J., 1993. Alluvial architecture in a sequence stratigraphic
1290 framework: a case history from the Upper Cretaceous of Southern Utah, USA. In: Flint,
1291 S.S., Bryant, I.D. (Eds.), The Geological Modelling of Hydrocarbon Reservoirs and
1292 Outcrop Analogues. Quantitative Modelling of Clastic Hydrocarbon Reservoirs and
1293 Outcrop Analogs. IAS Spec. Pub., pp. 21–55.

1294 Shanley, K.W., McCabe, P.J., 1994. Perspectives on the Sequence Stratigraphy of Continental
1295 Strata1. AAPG Bull 78 (4): 544–568

1296 Simon, S.S.T, Gibling, M.R., DiMichele, W.A., Chaney, D.S., Koll, R., 2018. An exhumed
1297 fine-grained meandering channel in the lower Permian Clear Fork Formation, north-central
1298 Texas: Processes of mud accumulation and the role of vegetation in channel dynamics. IAS
1299 Spec. Publ. 48, 149-172.

1300 Soreghan, G.S., Soreghan M.J., Sweet D.E., Moore K.D., 2009. Hot Fan or Cold Outwash?
1301 Hypothesized Proglacial Deposition in the Upper Paleozoic Cutler Formation, Western
1302 Tropical Pangea. J. Sed. Res. 79, 7, 495-522.

1303 Soreghan, G.S., Soreghan, M.J., Hamilton, M.A., 2008. Origin and significance of loess in
1304 late Paleozoic western Pangaea: A record of tropical cold?, Palaeogeogr. Palaeocl. 268,
1305 234-259.

1306 Soreghan, G.S., Sweet D.E., Heavens N.G., 2014a. Upland Glaciation in Tropical Pangaea:
1307 Geologic Evidence and Implications for Late Paleozoic Climate Modeling. J. Geol. 122
1308 (2), 137-163.

1309 Soreghan, M.J., Heavens, N., Soreghan, G.S., Link, P.K., Hamilton, M.A., 2014b. High-
1310 resolution record of Permian atmospheric circulation changes inferred from geochemical,
1311 magnetic, and sedimentologic indicators in the Maroon formation. Geol. Soc. Am. Bull.
1312 B30840, 1.

1313 Soreghan, G.S., Elmore, R.D., Lewchuk, M.T., 2002a. Sedimentologic–magnetic record of
1314 western Pangean climate in upper Paleozoic loessite (lower Cutler beds, Utah). Geol. Soc.
1315 Am. Bull. 114, 1019-1035.

1316 Soreghan, M.J., Soreghan, G.S., Hamilton, M.A., 2002b. Paleowinds inferred from detrital-
1317 zircon geochronology of upper Paleozoic loessite, western equatorial Pangea. Geology 30,
1318 695-698.

1319 Soreghan G.S., Beccaletto L., Benison K.C., Bourquin S., Hamamura N., Hamilton M.,
1320 Heavens N.G., Hinnov L., Huttenlocker A., Looy C., Pfeifer L.S., Pochat S., Sardar Abadi
1321 M., Zambito J., 2020. Report on ICDP Deep Dust workshops: Probing Continental Climate
1322 of the Late Paleozoic Icehouse-Greenhouse Transition and Beyond. Sci. Drilling 28, 93–
1323 112, https://doi.org/10.5194/sd-28-93-2020

1324 Stanesco, J.D., Dubiel, R.F., Huntoon, J.E., 2000. Depositional environments and
1325 paleotectonics of the Organ Rock Formation of the Permian Cutler Group, southeastern
1326 Utah. In: Sprinkel, D.A., Chidsey, T.C., Anderson, P.B (Eds), Geology of Utah's National
1327 Parks and Monuments. Utah Geol. Association Publ. 2, 591-605.

1328 Steele, B.A., 1987. Depositional Environments of the White Rim Sandstone Member of the
1329 Permian Cutler Formation, Canyonlands National Park, Utah. US Geol. Survey Bull. 1592,
1330 20.

1331 Sweet, M.L., 1999. Interaction between aeolian, fluvial and playa environments in the
1332 Permian Upper Rotliegend Group, UK southern North Sea. Sedimentology 46, 1, 171-187.

1333 Tabor N.J., Poulsen C.J., 2008. Palaeoclimate across the Late Pennsylvanian - Early Permian
1334 tropical palaeolatitudes: a review of climate indicator, their distribution, and relation to
1335 palaeogeographic climate factors. Palaeogeogr., Palaeocl., Palaeoec. 268, 293-310.

1336 Taggart, S., Hampson, G.J., Jackson, M.D., 2010. High-resolution stratigraphic architecture
1337 and lithological heterogeneity within marginal aeolian reservoir analogues. Sedimentology
1338 57, 1246-1279.

1339 Terrell, F.M., 1972. Lateral facies and paleoecology of Permian Elephant Canyon Formation,
1340 Grand County, Utah. Brigham Young Univ. Geol. Studies 19, 3–44.

1341 Tirsgaard, H., Øxnevad, I.E.I., 1998. Preservation of pre-vegetational fluvio-aeolian deposits
1342 in a humid climatic setting: an example from the Middle Proterozoic Eriksfjord Formation,
1343 southwest Greenland. Sed. Geol. 120, 295-317.

1344 Trewin, N.H., 1993. Controls on fluvial deposition in mixed fluvial and aeolian facies within
1345 the Tumblagooda Sandstone (Late Silurian) of Western Australia. Sed. Geol.85, 1-4, 387-
1346 400.
1347 Van Wagoner, J.C., Mitchum, R., Campion, K., Rahmanian, V., 1990. Siliciclastic Sequence
1348 Stratigraphy in Well Logs, Cores, and Outcrops: Concepts for High-Resolution Correlation
1349 of Time and Facies. AAPG Methods in Exploration Series 7, 55.
1350 Van Wagoner, J.C., Posamentier, H.W., Mitchum, R.M., Vail, P.R., Sarg, J.F., Loutit, T.S.,
1351 Hardenbol, J., 1988. An overview of the fundamentals of sequence stratigraphy and key
1352 definitions. In: Wilgus, C.K., Hastings, B.S., Kendall, C.G.St.C., Posamentier, H.W., Ross,
1353 C.A., Van Wagoner, J.C. (Eds), Sea-level changes: an integrated approach. SEPM Spec.
1354 Publ. 42, pp. 39-45.
1355 Vaughn, P.P., 1964. Vertebrates from the Organ Rock Shale of the Cutler Group, Permian of
1356 Monument Valley and vicinity, Utah and Arizona. J. Paleont. 567-583.

1357 Veiga, G.D., Spalletti, L.A., Flint, S., 2002. Aeolian/fluvial interactions and high-resolution
1358 sequence stratigraphy of a non-marine lowstand wedge: the Avilé Member of the Agrio
1359 Formation (Lower Cretaceous), central Neuquén Basin, Argentina. Sedimentology 49, 5,
1360 1001-1019.

1361 Venus, J.H., Mountney, N.P., McCaffrey, W.D., 2015. Syn-sedimentary salt diapirism as a
1362 control on fluvial-system evolution: an example from the proximal Permian Cutler Group,
1363 SE Utah, USA. Bas. Res. 0, 1-31.

1364 Wakefield, O.J.W, Mountney, N.P., 2013. Stratigraphic architecture of back-filled incised-
1365 valley systems: Pennsylvanian–Permian lower Cutler beds, Utah, USA. Sed. Geol. 298, 1-
1366 16

1367 Wanless, H.R., Shepard, F.P., 1936. Sea level and climatic changes related to late Paleozoic
1368 cycles. Geol. Soc. Am. Bull., 47, 8, 1177-1206.
1369 Wengerd, S.A., Matheny, M.L., 1958. Pennsylvanian system of the four corners region.
1370 AAPG Bull. 42, 9, 2048-2106.

1371 White, D., 1929. Flora of the hermit shale, Grand Canyon, Arizona. Carnegie Instit.
1372 Washington Publ. 405, 221.

1373 Wright, P.V., Marriott, S.B., 1993. The sequence stratigraphy of fluvial depositional systems:
1374 the role of floodplain sediment storage. Sed. Geol. 86, 203–210.

1375 Wyżga, B., Mikuś, P., Zawiejska, J., Ruiz-Villanueva, V., Kaczka, R.J., Czech, W., 2017. Log
1376 transport and deposition in incised, channelized, and multithread reaches of a wide
1377 mountain river: Tracking experiment during a 20-year flood. Geomorphology 279, 98-111.
1378 Yang, C.H., Nio, S.D., 1993. Application of high-resolution sequence stratigraphy to the
1379 Upper Rotliegend in the Netherlands offshore. In: Weimer, P., Posamentier, W. (Eds),

Siliciclastic sequence stratigraphy, recent developments and applications. AAPG Mem. 58, pp. 285-316.

Figure captions

Fig. 1. (A) Location of the studied area; (B) schematic palaeoenvironmental map of the Utah state from Lawton et al. (2021) blue is marine, brown is continental; (C) location of the sections in the Paradox Basin and major paleo-reliefs (modified from Condon, 1997).

Fig. 2. Main lithostratigraphic units in Canyonlands area. Nomenclature of Baars (1962) and Loope (1984). See Fig. 1 for location.

Fig. 3. Outcrops of A) Hurrah Pass section; B to D) Potash Road; E to G) Lockhart Canyon section; H to J) Elephant Hill section inside park; K, L) Elephant Hill section outside park; M) Cathedral Butte section. See Fig. 1 for the location.

Fig. 4. Sedimentological section at Hurrah Pass with interpretations as depositional environments and sequence stratigraphy. See Figs. 1 and 3A for the section location.

Fig. 5. Sedimentological section at Potash Road with interpretations as depositional environments and sequence stratigraphy. See Figs. 1 and 3B to D for the section location.

Fig. 6. Sedimentological section at Lockhart Canyon with interpretations as depositional environments and sequence stratigraphy. See Figs. 1 and 3E to G for the section location.

Fig. 7. Sedimentological section at Elephant Hill with interpretations as depositional environments and sequence stratigraphy. See Figs. 1 and 3H to L for the section location.

Fig. 8. Sedimentological section at Cathedral Butte with interpretations as depositional environments and sequence stratigraphy. See Figs. 1 and 3M for the section location.

Fig. 9. Aeolian facies: A) Overview of the facies association E1 showing stacked AT facies, trough cross-bedded aeolian sandstones, Cathedral Butte (from 0 to 20 m, Fig. 8); B) Detail of contorted bedding in the facies AT; C) Detail of the facies Ar (location on photography F): subcritical climbing translatent stratification, horizontal to low-angle cross-lamination with inverse grading; D) Facies AT: trough cross-bedded sandstones with grainfall lamination and grainflow (avalanche) strata, Elephant Hill; E) Facies Ah, aeolian sand-sheet; F) E1 and E3 facies association of the White Rim Sandstone at the top of Potash Road (Fig. 5) unconformably overlain by Triassic deposits; G) Facies association Aa, adhesion structure. H) Genetic units of the Organ Rock Fm at the Cathedral Butte section (Figs. 3M, 8) with detail of (I) the genetic units 34 and 35, and of J) bioturbations within E1 facies of these genetic units. See Tables 1, 2 for facies and facies association description.

Fig. 10. Alluvial facies: A) Facies St: trough cross-bedded sandstone; B) Facies St: trough cross-bedded sandstone with mud-clasts (white arrows); C) Overview of alluvial facies association, F1, F2: incised channel deposits with erosive basal boundary, Potash Road; D) Facies Sm, massive sandstone; E) Facies Sh facies, horizontal laminated sandstones; F) Facies Sm and Sh with mud-clasts, respectively massive and horizontal laminated sandstones; G) Facies Fl overlain by facies Sm and Sh; H) Facies Sh and F; I) Mudcracks, J) Facies Sr (ripple cross-laminated sandstones) within facies F; K) Facies Sm and F with pedogenetic nodules

(Pn); L) facies F, siltstones, with root traces (Pr); M) Facies Std and Shd respectively trough cross and horizontal bedding alternating with deflation lag surface (d); Alluvial facies association F1 (A to C), F2 (D to G), F3 (H to L) and FE (M). See Tables 1, 2 for facies and facies association description.

Fig. 11. Coastal facies: A) facies Stb: trough cross bedded sandstones bioturbated B) mainly by diplocraterion with frequently C) fluid escape structure; D) Facies Sb, bioturbated massive sandstone with *Planolites*; E) Facies Msig, tidal bar; F) Detail of facies Msig showing clay drapes; G) Facies Msig, tidal bar with hearing bones structures; H) Facies Srw, current and wave ripples; I) Heterolithic biourbated facies SFb; J) Facies Cf, sandy limestone or limestone with bioclasts; K) Brachiopod; L) Gastropods; M) Crinoids; N) Overview of the coastal facies association at Elephant Hill section (from 0 to 20 m, Figs. 3H, 7). See Tables 1, 2 for facies and facies association description.

Fig. 12. Subaqueous facies: A) Facies ST with contorted bedding; B) Detail of the base of the foreset of the facies ST with C) Facies Sb, bioturbated sandstone and D) Facies Srb, bioturbated current ripples; Facies association S2 with detail of E) facies SFb and FlB, of F) Facies Srb, bioturbated ripple cross-laminated sandstone and of G) Facies Fb and Sm; H) Overview of the marine (S1, S2, C3, C1) and alluvial (F1) facies association, Potash Road section (from 45 to 73 m, Figs. 3E, 5); I) Overview of marine (S2, C1 and C2) and aeolian facies (E1 association), Hurrah Pass section (from 105-118m, Figs. 3A, 4). See Tables 1, 2 for facies and facies association description.

Fig. 13. (A) Comparison between aeolian dunes and longshore dunes; (B) Detail of the stacking of aeolian dunes separated by root traces, and aeolian dunes overlain by longshore bar (Cathedral Butte section from 43 to 56 m, Fig. 8).

Fig. 14. Schematic representation of the different depositional environments identified in the Late Pennsylvanian to the early Permian sections of the Canyonlands National Park (Fig. 1).

Fig. 15. Genetic units observed in the Late Pennsylvanian to the early Permian sections of the Paradox Basin. Two type of genetic unit are observed: (A) type 1, without aeolian deposit and (B) type 2 with aeolian deposits preservation. The progradational phase is rarely complete and some facies are missing (C, D). The retrogradational phase is rarely preserved implying sometimes an abrupt transition from longshore bar to aeolian dune facies, sometimes underlain by root traces (E), or by evidence of colonisation by organisms that burrow vertically into the substrate (F). See explanation in the text.

Fig. 16. Panorama of the Lockhart Canyon section (A) where the sedimentological section has been realized (from 30 to 90 m; Fig. 6) and (B) a lateral equivalent; (C, D) Panorama of Elephant Hill section outside park (from 110 to 165 m, Figs. 3K, 7).

Fig. 17. Correlations at the scale of the study area. See Fig. 1 for the section location and Figs. 4 to 8 for detail sedimentological sections.

Fig. 18. Landscape evolution of the Paradox basin during the Late Pennsylvanian to the early Permian inferred from the sedimentological analyses and correlations of the studied section with a) First step (cycles I to V, Fig. 17); b) Second step (cycles VI to XI, Fig. 17) and c) Third step (cycles XII to XIV, Fig. 17).

Fig. 19. Stratigraphic cycles in relation with sea-level variations.

Fig. 20. A model of the genetic unit evolution in the coastal environment of the central Pangean equatorial region during Late Pennsylvanian-early Permian glacial world. See explanation in the text and Fig. 19.

Table 1. Facies description: code facies, lithology, bioturbation and fossil content, sedimentary structures and their interpretation in terms of depositional process.

Table 2. Facies Associations: code of the facies association, sedimentary architecture and their interpretation in terms of depositional environments. Paleocurrents measured in each facies association are also represented. See Table 1 and Supplementary Data Figs. 2, 3, respectively for facies, bioturbation and root traces.

Supplementary Data captions

Supplementary Data Fig. 1. Correlation surfaces from Google Earth images; Surface D, purple line: between Hurrah Pass, Potash Road, Lockhart Canyon and Elephant Hill sections (Figs. 3, 4 to 7, and 17); Yellow line: between the Elephant Hill section inside and outside of the park (Fig. 3 and noted 2 Fig. 7); Surface E, orange line: between Elephant Hill and Cathedral Butte sections (Figs. 3, 7, 8 and 17).

Supplementary Data Fig. 2. Bioturbations: A) *Diplocraterion*: A1 top view, A2 section view; B) *Palaeophycus*: B1 top view, B2 section view; C) *Planolites*: C1: top view, C2 section view; D) *Scolicia*: top view); E) *Thalassinoides*: E1 top view, E2 section view; F) *Psilonichnus*; G) *Taenidium*: G1, Hymenopter trackways, G2 Coleopteran trackways.

Supplementary Data Fig. 3. Root traces and wood: A) Calcrete Pn; B) Thin and short root traces Pr, in siltstones (B1) or sandstones (B2), or associated with carbonate nodule and concretion, Prn (B3); C) Long and large root traces usually observed in sandstones (C3) and sometimes in fine-grained facies with carbonate concretion (C1, C2, lower Cutler beds at Elephant Hill); D) Long and large root traces with preserved wood, PRmo at Hurrah Pass, at top of aeolian dunes (D1) or at the top of subaqueous dunes (D2, D3); E) Stump horizon with cornaline fillings at the top of the lower Cutler beds Fm at Potash Road (E1) and stump horizon at the top of the Cedar Mesa Sandstone at Cathedral Butte (E2, E3); F) Fossil wood: at the base of the lower Cutler beds at Potash Road either interbedded within St facies (F1), or 20 m-long trunk (F4), at the top of the lower Cutler beds isolated within fine-grained facies (F2), or at the top of the Cedar Mesa Sandstone at Cathedral Butte (F3).

Supplementary Data Fig. 4. Thin section showing of composition of A) marine (LB37: Lockhart Canyon section at 37 m, Fig. 7) and B) aeolian sandstones (CB8, CB58, CB107: Cathedral Butte section respectively at 8 m, 58 m and 107 m, Fig. 8; EH58: Elephant Hill at 58 m, Fig. 7). See explanation in the text.

Figure1

Click here to access/download;Figure;Fig1.pdf

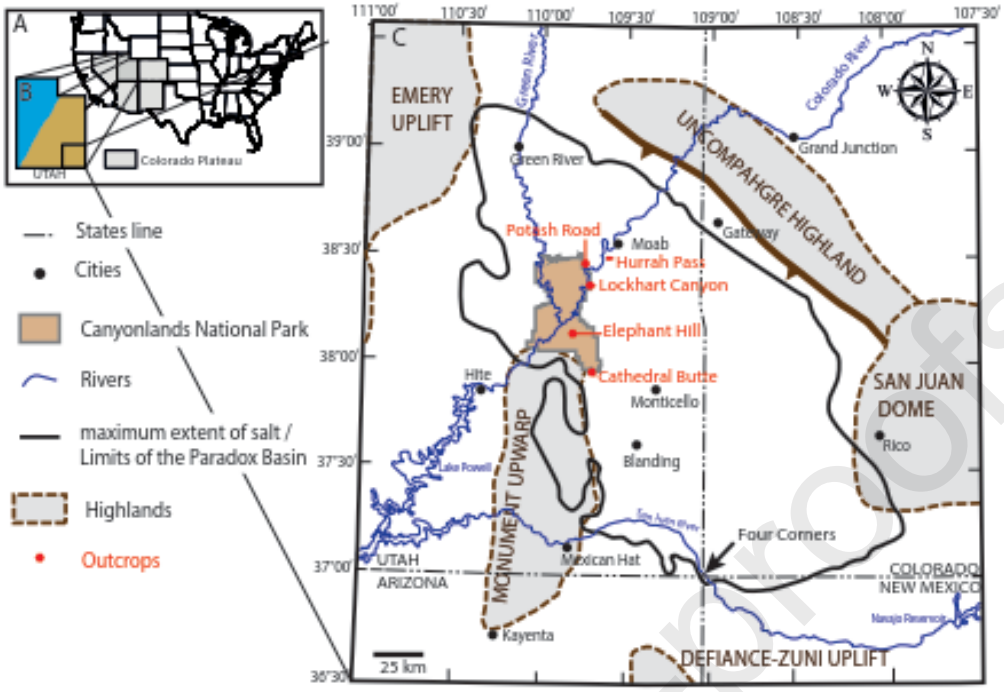

1501

1502

1503

Figure2

Click here to access/download;Figure;Fig2.pdf

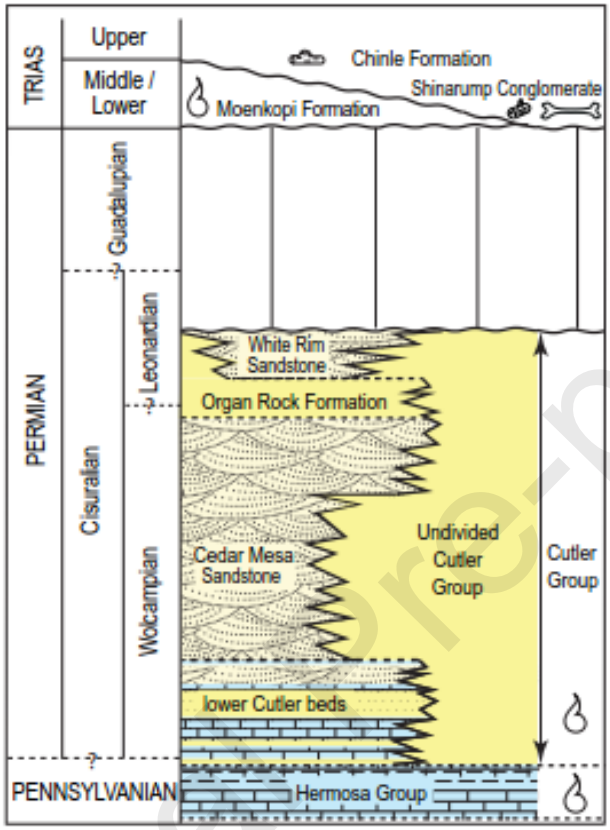

1504

Figure3

Click here to access/download;Figure;Fig3.jpg

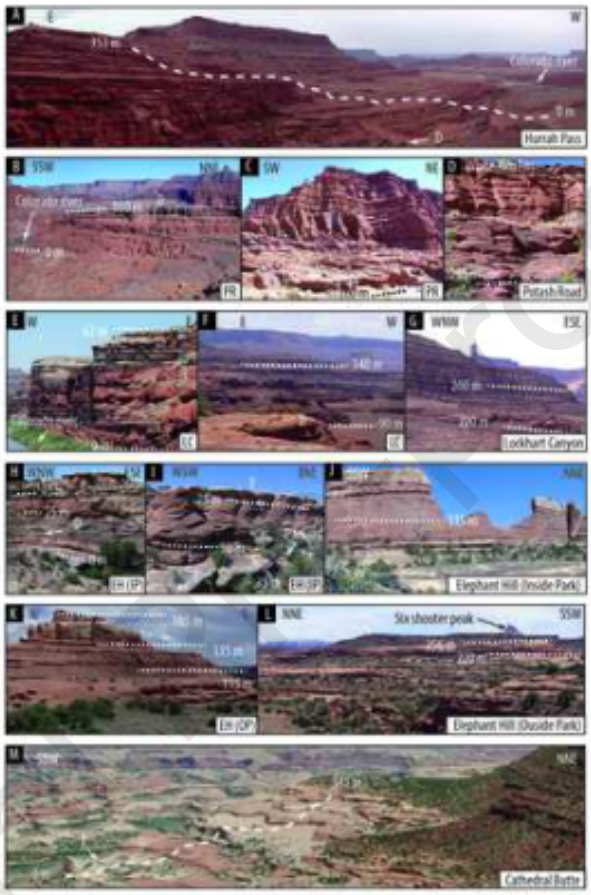

1505

1506

Figure4

Click here to access/download;Figure;Fig4.pdf

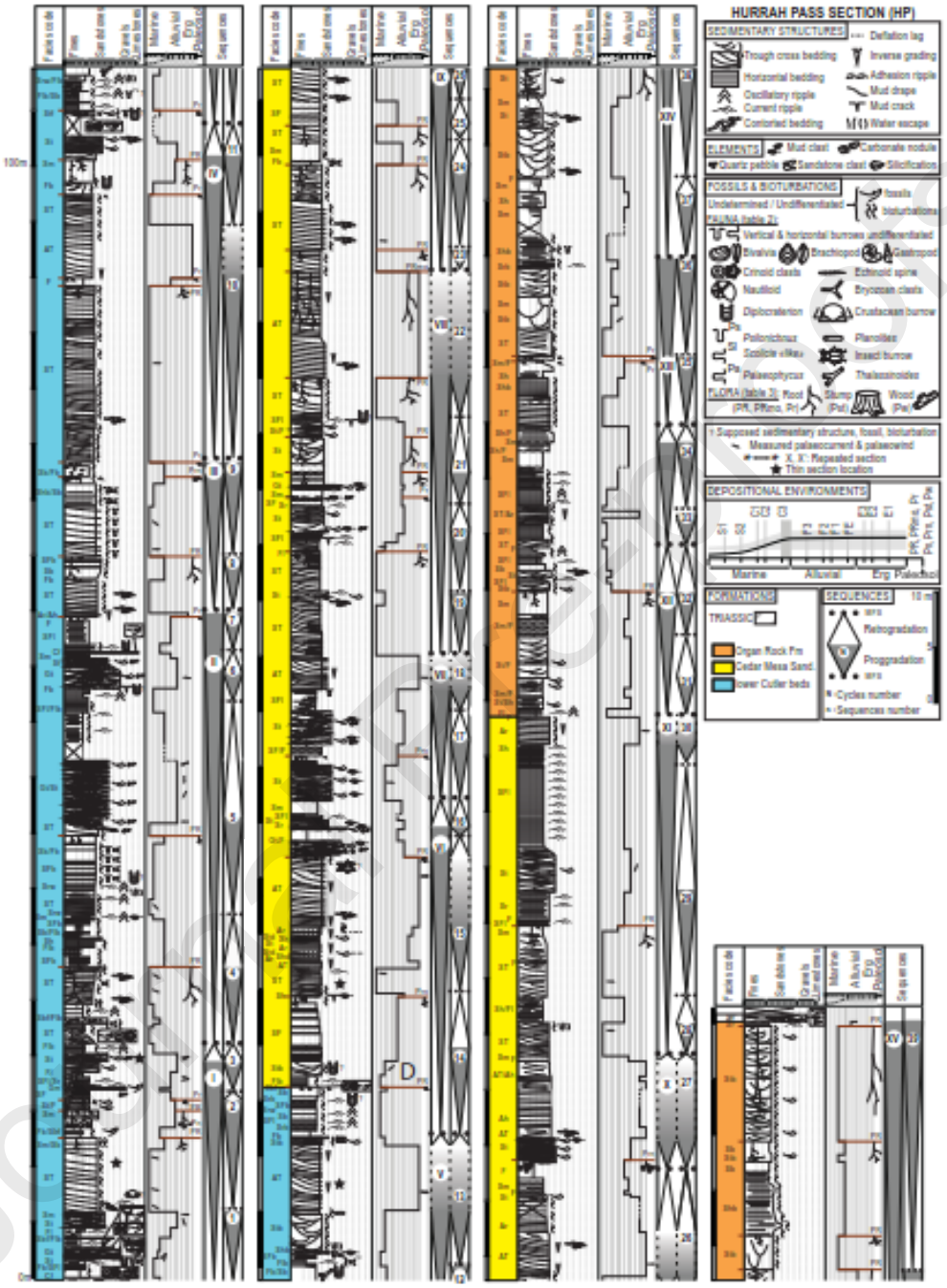

1507

1508

Figure5

Click here to access/download;Figure;Fig5.pdf

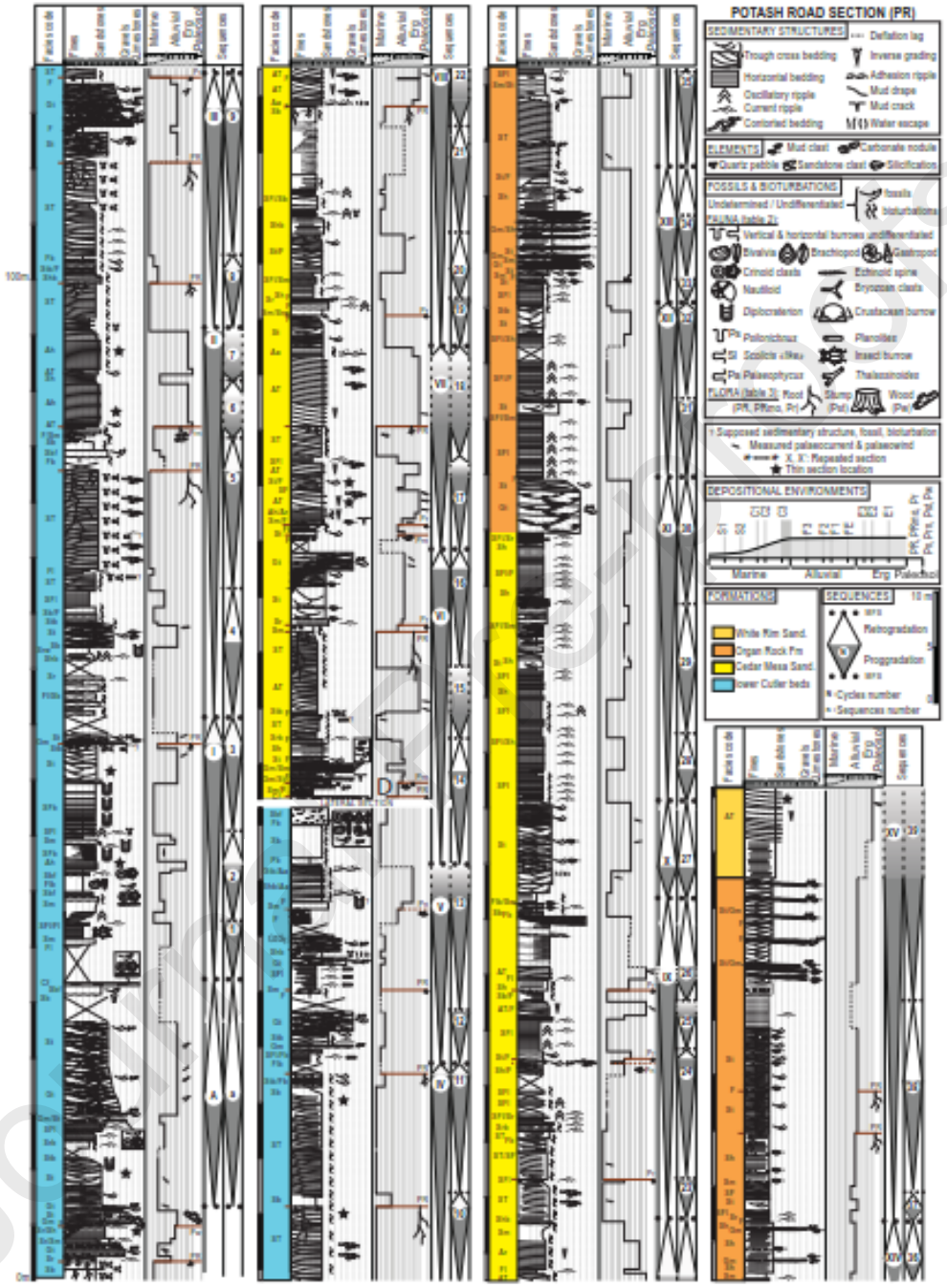

1509

1510

Figure6

Click here to access/download;Figure;Fig6.pdf

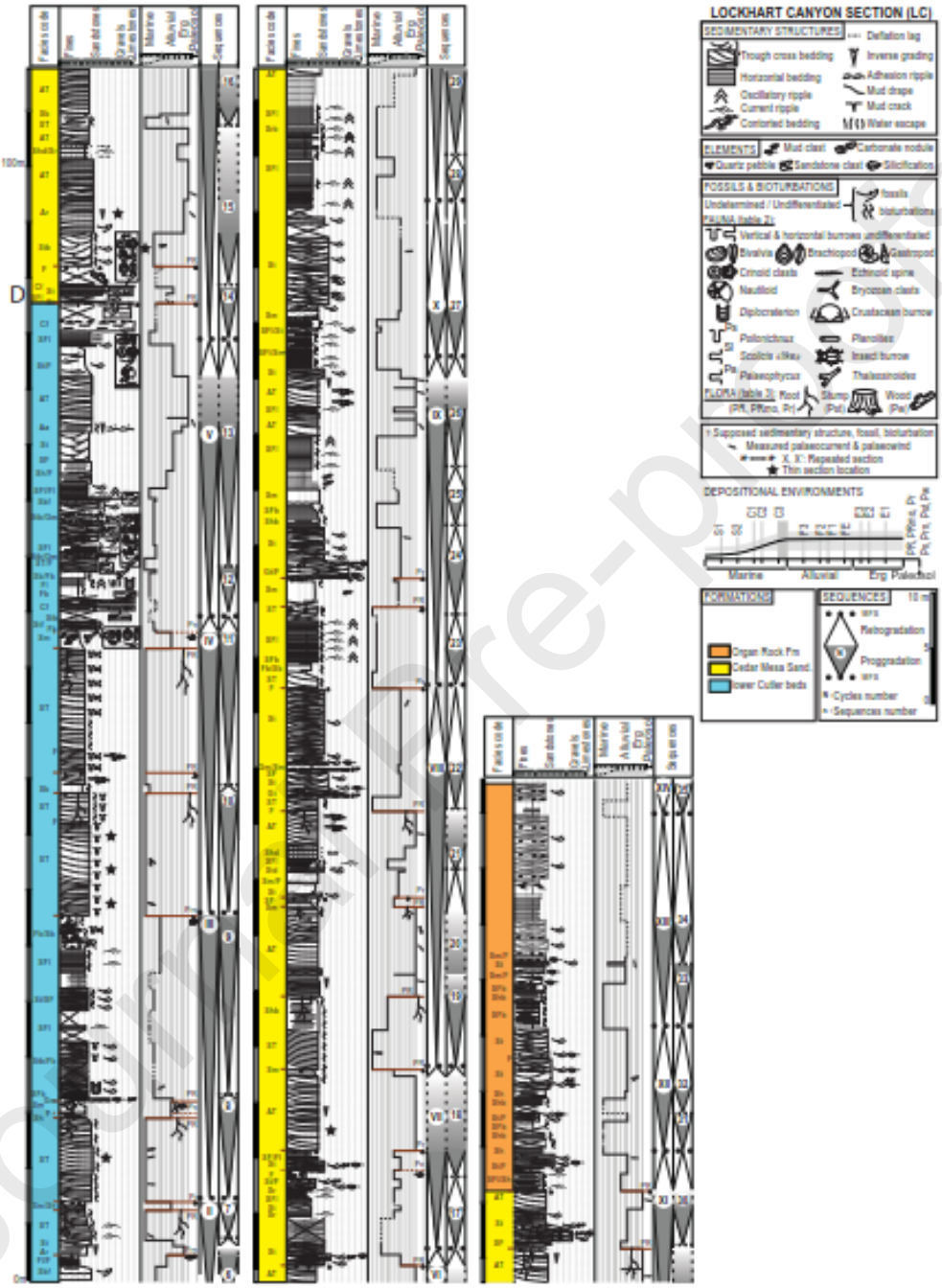

1511

1512

Figure7

Click here to access/download;Figure;Fig7.pdf

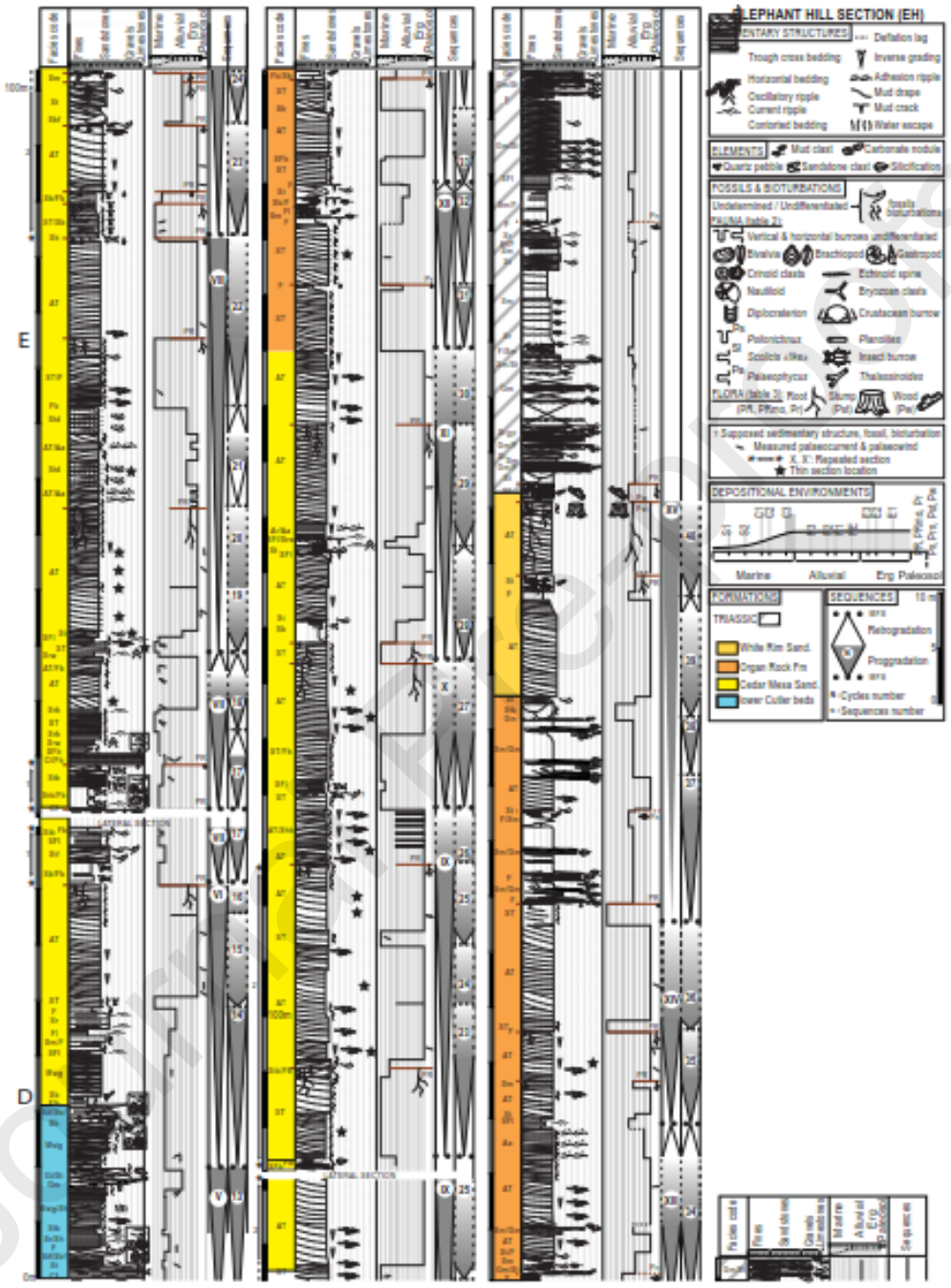

1513

Figure8

Click here to access/download;Figure;Fig8.pdf

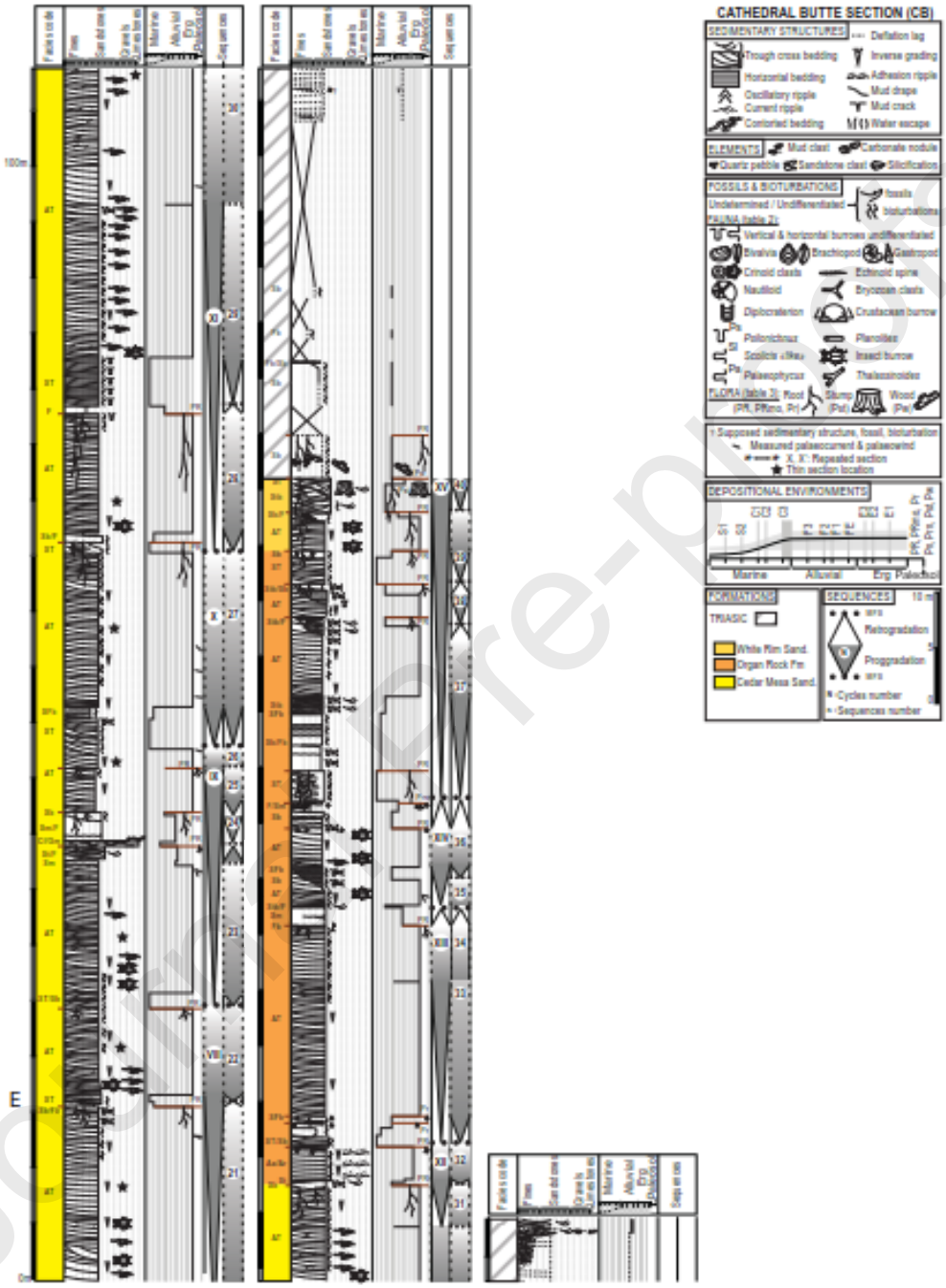

1514

1515

Figure9

Click here to access/download;Figure;Fig9.jpg

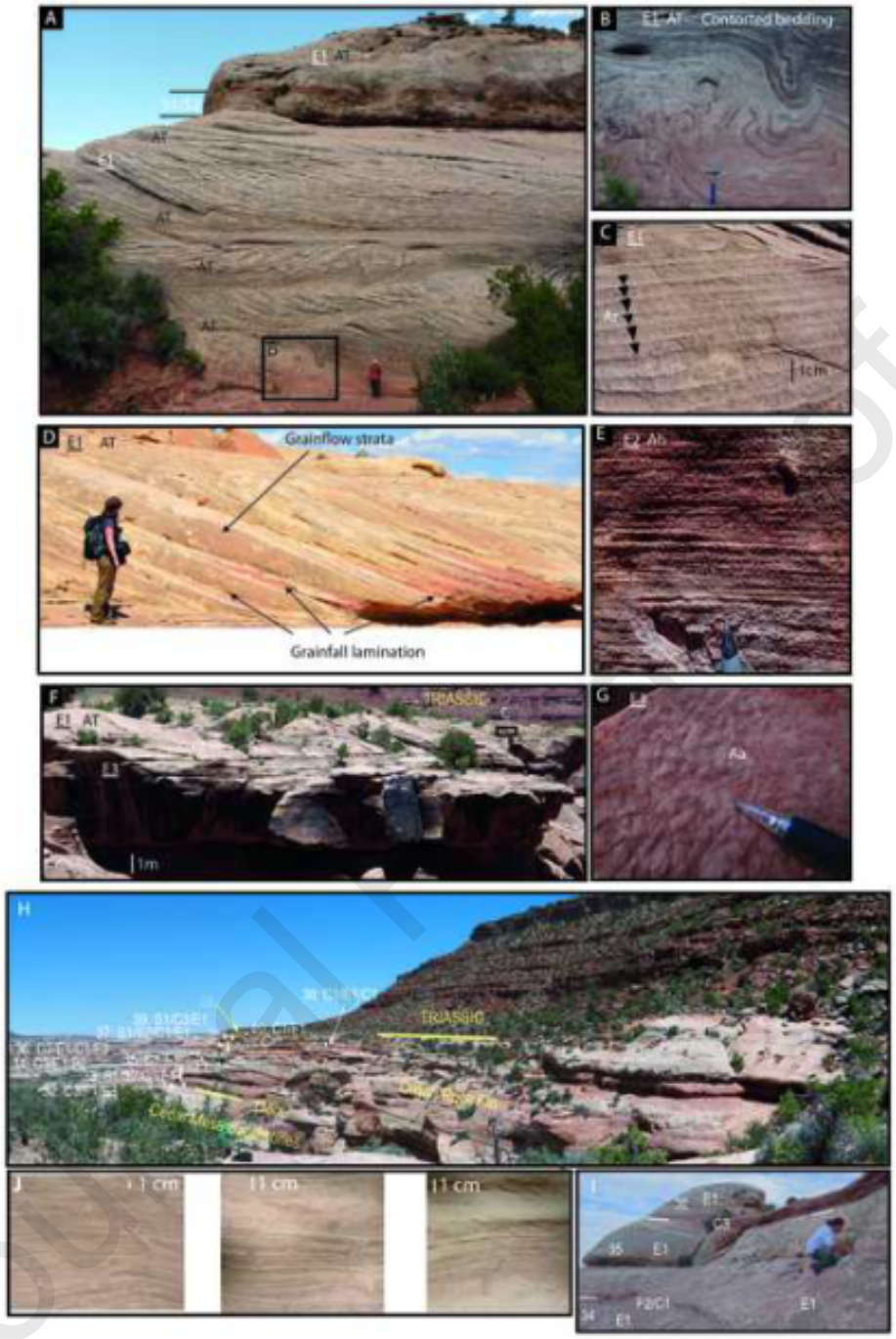

1516

1517

Figure10

Click here to access/download;Figure;Fig10.jpg

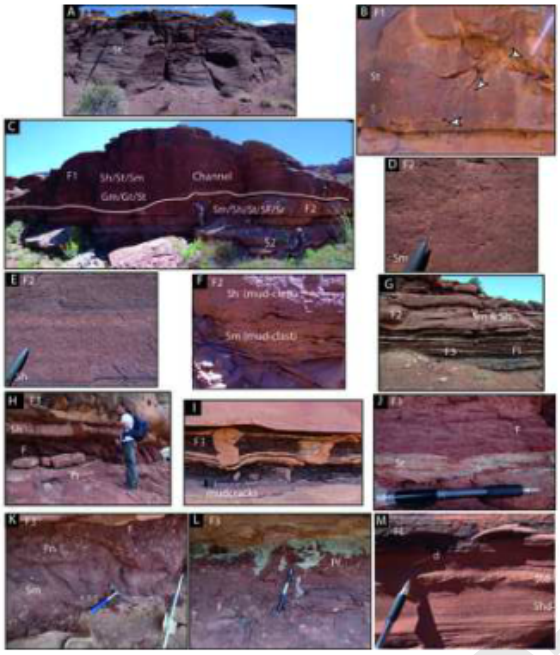

1518

1519

Figure11

Click here to access/download;Figure;Fig11.jpg

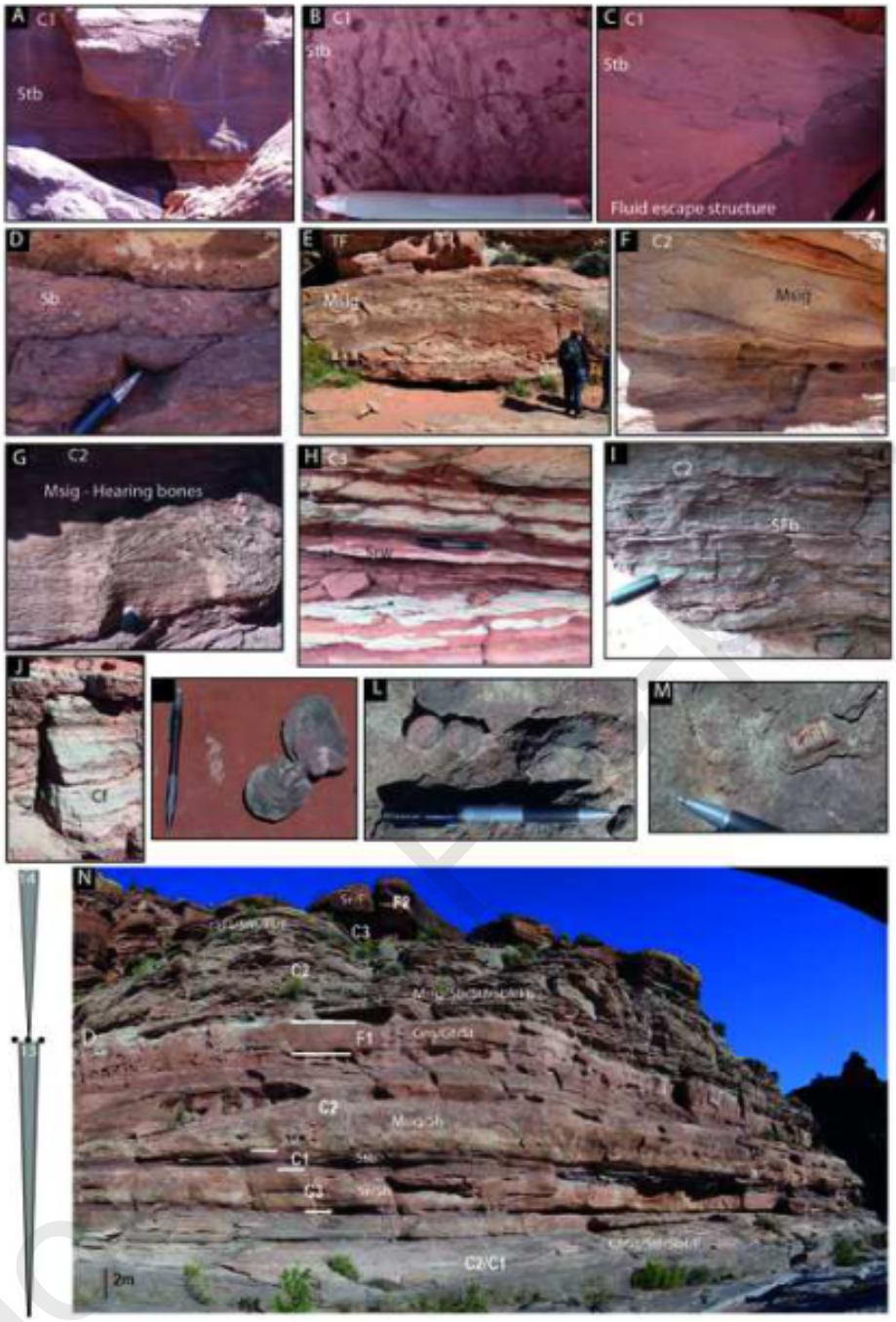

1520

1521

Figure12

Click here to access/download;Figure;Fig12.jpg

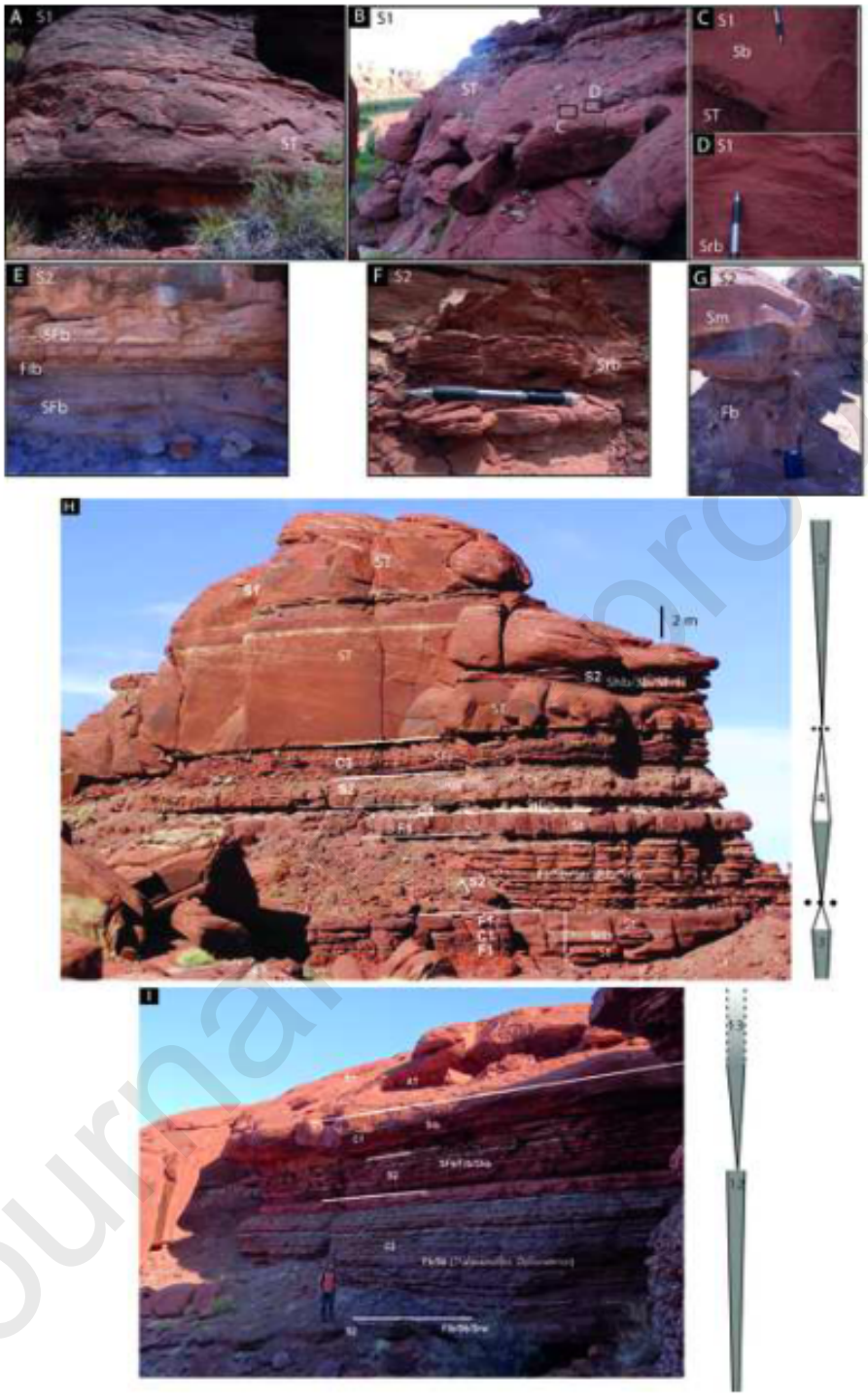

1522

1523

Figure13

Click here to access/download;Figure;Fig13.jpg

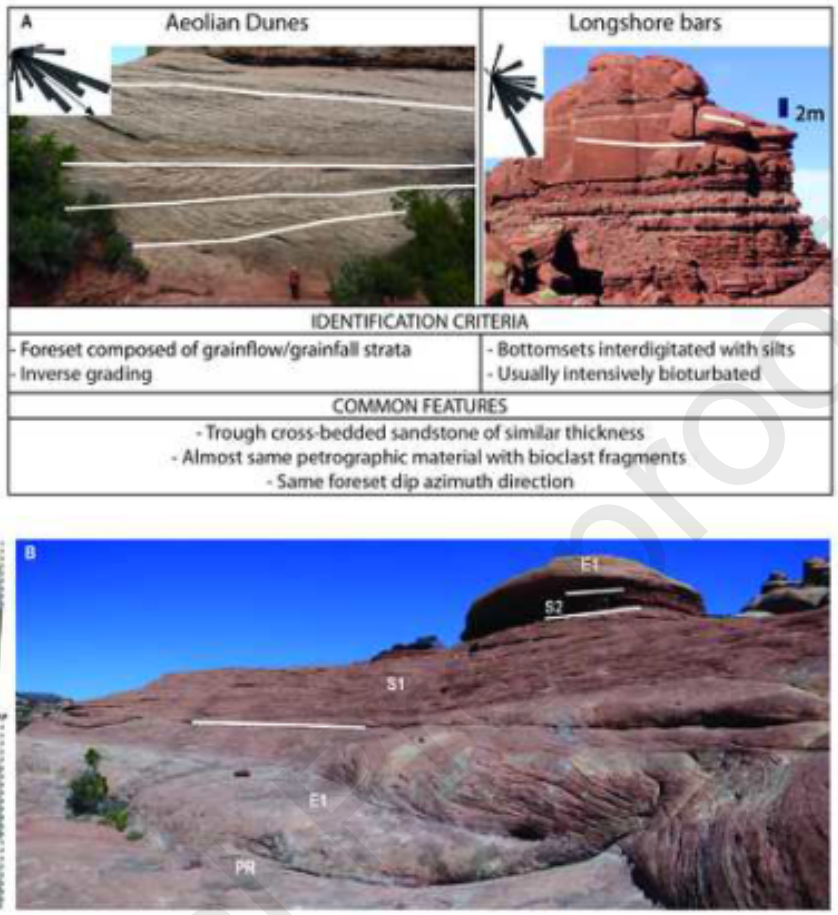

1524

1525

Figure14

Click here to access/download;Figure;Fig14.jpg

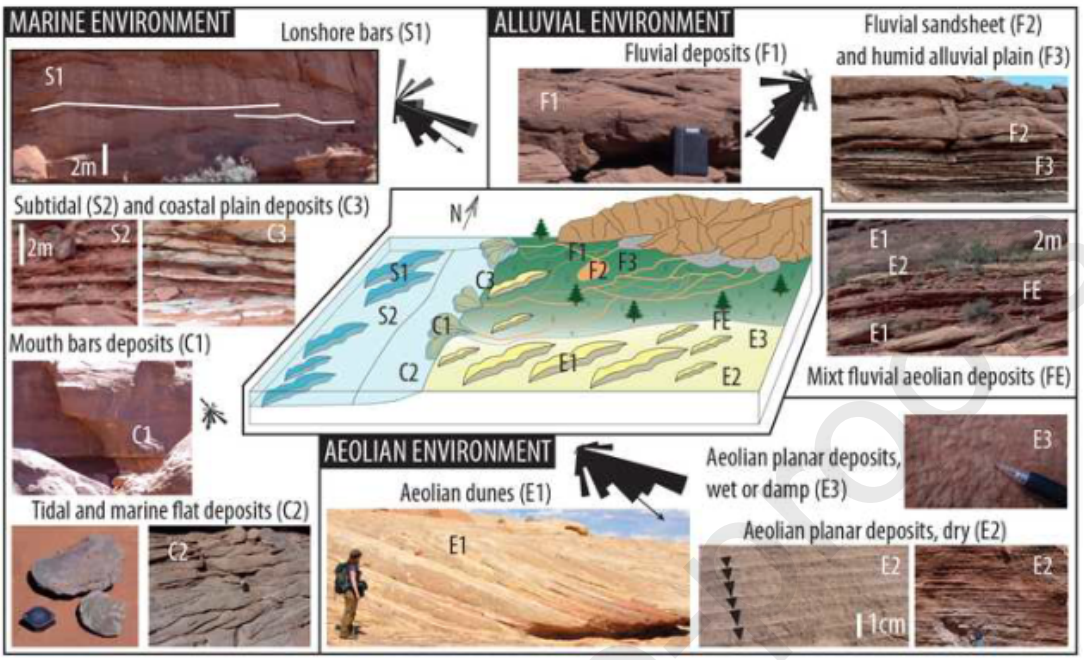

1526

1527

Figure15

Click here to access/download;Figure;Fig15.pdf

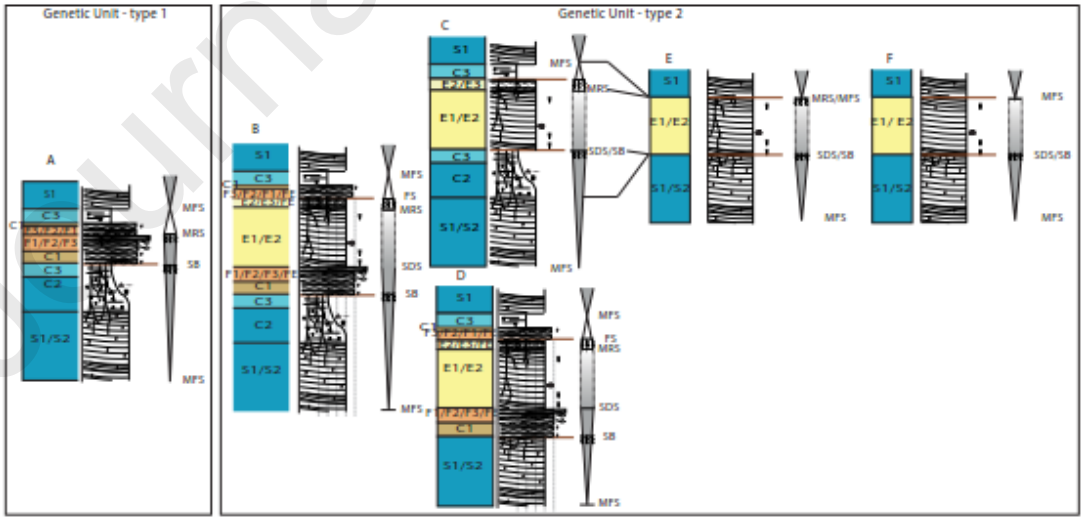

1528

1529

Figure16

Click here to access/download;Figure;Fig16.jpg

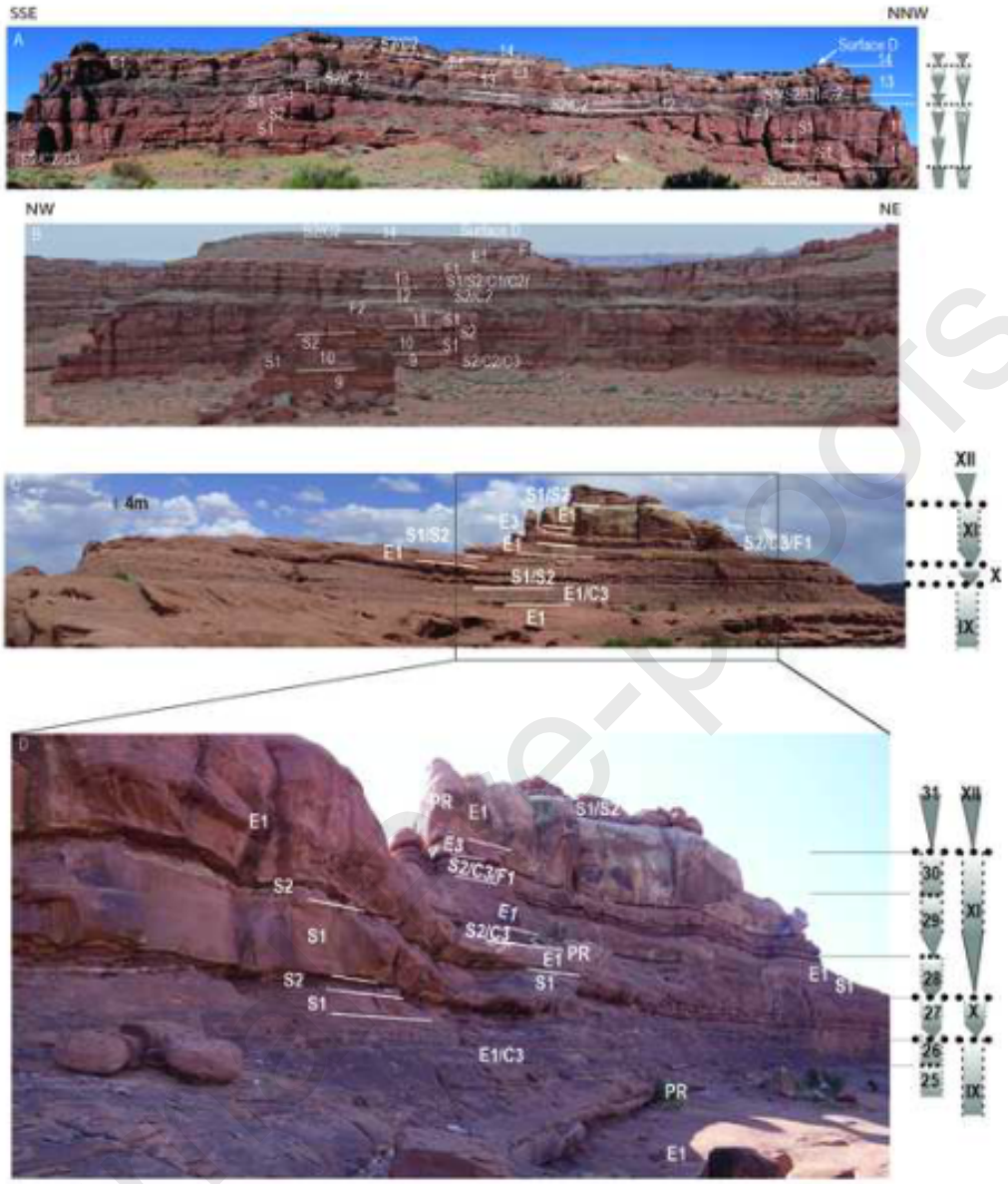

1530

1531

Figure17

Click here to access/download;Figure;Fig17.pdf

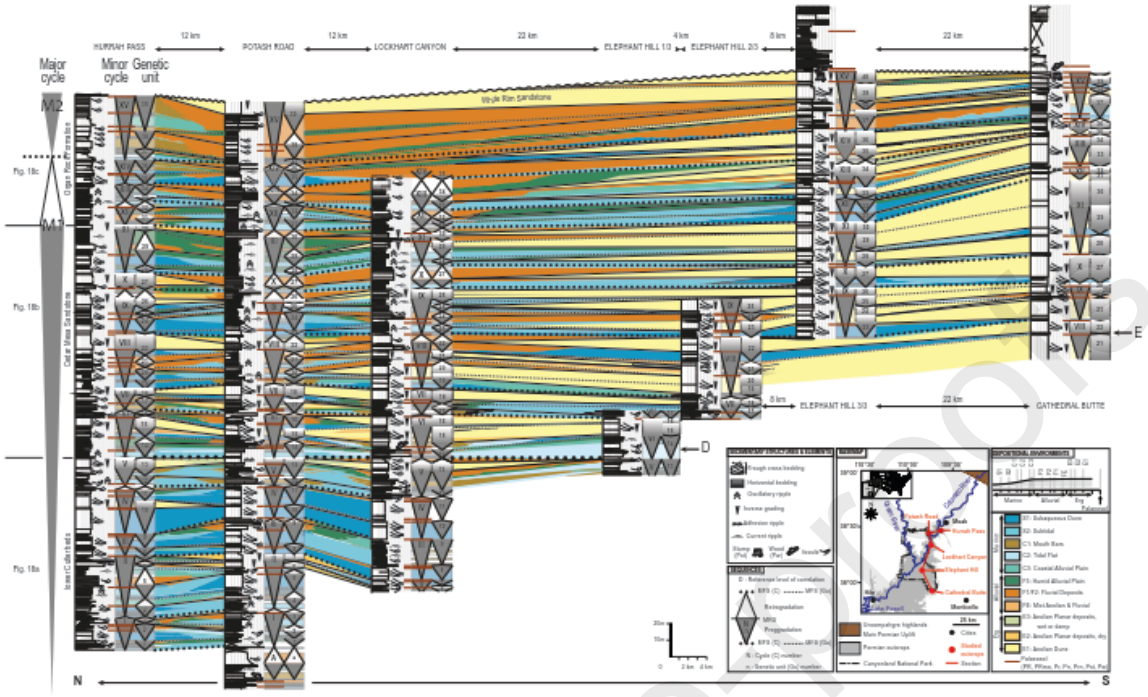

1532

1533

Figure18

Click here to access/download;Figure;Fig18.pdf

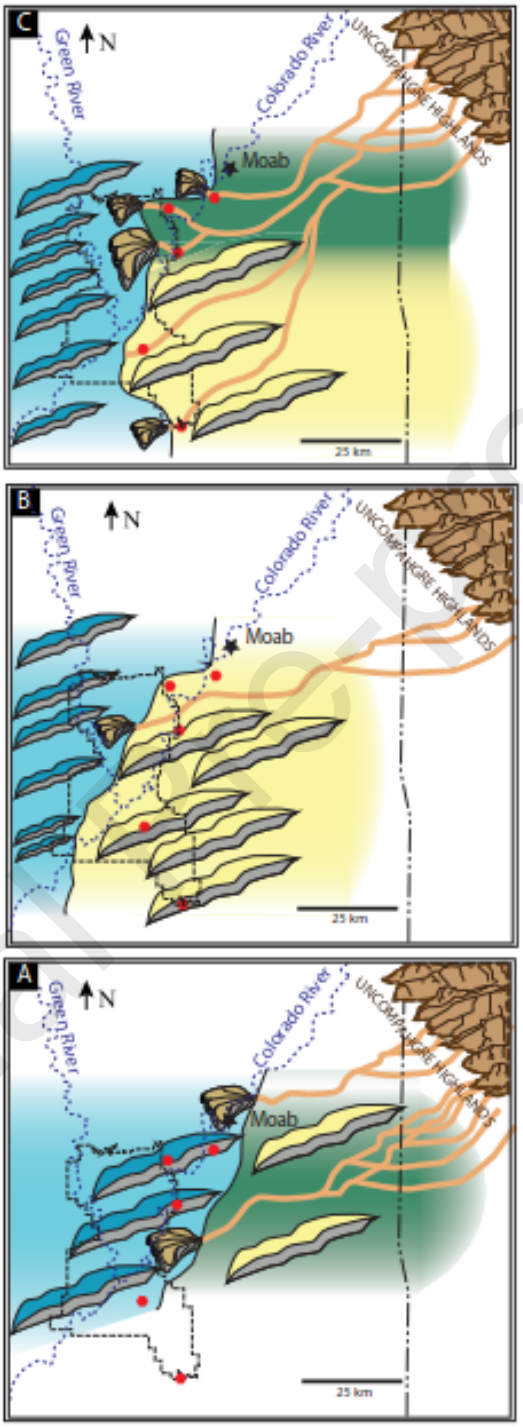

1534

1535

Figure20

Click here to access/download;Figure;Fig20.jpg

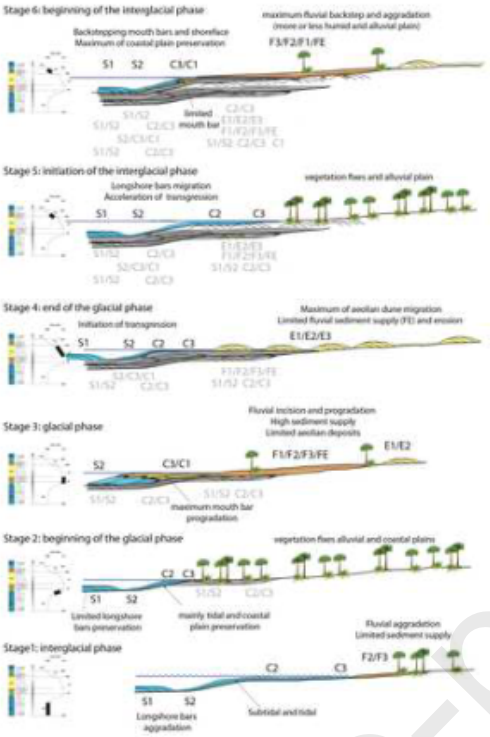

1536

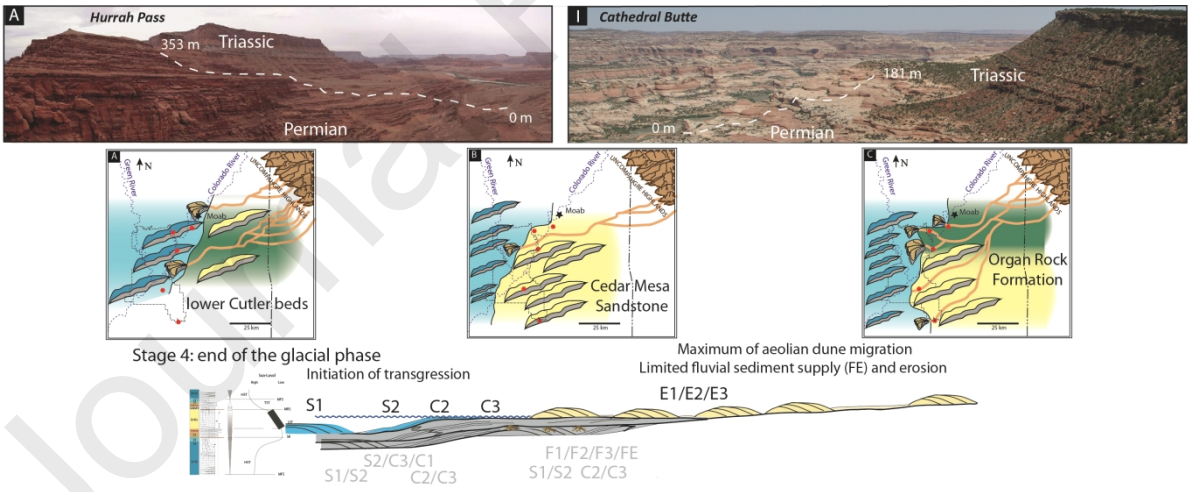

1537

1538 Highlights

1539

1540 • High-resolution sequence stratigraphic in aeolian and coastal environment
1541 • Stratigraphic cycle and vegetation taphonomy within glacial-interglacial phases
1542 • Landscape evolution of the early Permian succession in western Equatorial Pangea

1543

Credit author statement

Marie Olivier: Funding acquisition on the field, writing original draft

Sylvie Bourquin: Funding acquisition, writing original draft and review, supervisor

Guy Desaubliaux: Funding acquisition on the field, writing-review, co-supervisor

Celine Ducassou: Funding acquisition on laboratory (petrographic analysis), writing-review

Camille Rossignol: Funding acquisition on the field, writing-review

Gautier Daniau: Funding acquisition on the field, writing-review

Dan Chaney: Funding acquisition on the field (paleobotanist), writing-review

Declaration of interests

☒ The authors declare that they have no known competing financial interests or personal relationships that could have appeared to influence the work reported in this paper.

☐ The authors declare the following financial interests/personal relationships which may be considered as potential competing interests:

Code	Lithology	Bioturbation (Ichnotaxa) & Fossil	Sedimentary structure	Depositional process
Conglomerates				
Gm Conglomerates	Angular to sub-rounded gravels to boulders (0.4 mm up to 20	Very rarely indeterminate fossils, crinoid fragments, bivalves,	Massive, Erosive basal boundary	Lag deposits or debris flow (Miall, 1996; Postma, 1990)

	cm), polygenic clasts (sandstones, quartz grains, claystones, basement and carbonate rock fragments), poorly sorted, matrix supported (very-fine to coarse sand) Beds thickness: 5 cm to 2 m	gastropods		
Gt Trough cross-bedded conglo merates	Same lithology than the Gm facies with occasionally huge wood clasts (up to 3m high) Beds thickness: 10 cm to 4.5 m	Very rarely indeterminate fossils, crinoid fragments	Through cross stratifications (h=10cm to 1.5m, λ=m to dam) Erosive basal boundary	Tractive current, upper part of the lower flow regime, 3D megaripple migration of fluvial or mouth bar deposits (Miall, 1978)
Sandstones				
AT Aeolian trough cross-bedded sandsto nes	Fine- to medium-grained sand, well-sorted and usually well-rounded sands Beds thickness: 20 cm to 5 m	Indeterminate bioturbation, *Taenidium,* Hymenopter, Coleoptera burrows, nests (Supplementa ry Data Fig. 3G)	Trough cross-bedded sandstones (h=20 cm to 5 m, λ=several m to dam, angles of dip: 10° to 31°) composed of grainfall laminations and grainflow (tongue-like avalanche), foresets are frequently draped	Aeolian dunes with avalanches on dune leeside, grainfalls in zone of flow separation (Hunter, 1977; Clemmensen & Abrahamsen, 1983; Brookfield & Silvestro, 2010), and subcritical climbing translatent stratification (scts), i.e. wind ripples (Hunter, 1977)

		at the base by inverse climbing ripples (Fig. 9A, C, D, F). Sharp basal boundary Occasional contorted bedding, small syn-sedimentary faults (cm to 1m) and small avalanches (Fig. 9B)	
Ar Translatent strata / wind ripple-laminated sandstones	Fine- to medium-grained sand, well-sorted and usually well-rounded sands Beds thickness: 5 cm to 3 m	Horizontal and low-angle mm-scale laminations composed inverse grading sand (Fig. 9C)	Migration of wind ripples (scts, Hunter, 1977)
Ah Aeolian Sandsheet	Fine- to medium-grained sand, well-sorted and usually well-rounded sands Beds thickness: 5 cm to 3.5 m	Horizontal and sub-horizontal laminations underlain by well-sorted and rounded quartz grains, “millet seed” texture (Fig. 9E) Sharp basal boundary	Tractional deposition by high velocity wind (Hunter, 1977; Clemmensen & Abrahamsen, 1983)
Aa	Fine- to medium-	Irregular horizontal and sub-horizontal	Wind-blown sand sticking to a wet or

Adhesion structures	grained sand, well-sorted and usually well-rounded sands Beds thickness: 5 cm to 2.5 m	mm-scale laminations composed of adhesion warts and ripples, and rarely discontinue inverse grading laminations (Kocurek & Fielder, 1982; Brookfield, 1992) (Fig. 9G) Sharp basal boundary	damp surface (Kocurek & Nielson, 1986; Brookfield & Silvestro, 2010)
St Trough cross-bedded sandstones (Fig. 10A)	Very fine- to coarse-grained sand, laminations occasionally underlined by gravels of quartz and/or mud-clasts (Fig. 10B) and more rarely by sandstones, basement, carbonates or wood clasts (Supplementary Data Fig. 2F1), poorly sorted Locally well-preserved big trees (> 20 m long and up to 60 cm of diameter; Supplementary Data Fig. 2F4) are present Beds thickness: 20 cm to 8 m	Trough cross stratifications (h=10 cm to 1 m, λ=m to dam), Ungraded or normally-graded Erosive or rarely sharp basal boundary Occasionally deformed beds and perturbed laminations (tectonic movements during or just after sedimentations) and contorted bedding (post depositional soft sediment deformation)	Tractive current, upper part of the lower flow regime, 3D megaripple migration, fluvial or mouth bar deposits (Miall, 1978)

Sh Horizontal laminated sandstones (Fig. 10E)	Very fine to medium sand and calcareous cement Beds thickness: 20 cm to 2 m	Horizontal laminations, occasionally underlain by mud-clast (Fig. 10F) Erosive and sharp basal boundary Ungraded or normally-graded	Upper flow regime (Miall, 1978), sheet-flood at a relative shallow depth or at the top of mouth bar (Pollard et al., 1982; Marshall, 2000; Hinds et al., 2004)
Std Trough cross-bedded sandstones with deflation surfaces	Fine- to medium-grained sand, well-sorted, rounded quartz grains Beds thickness: 20 cm to 2.5 m	Trough cross stratifications of fine sand (h=10 cm to 40 cm, λ=m) alternating with horizontal to sub-horizontal surfaces of "millet seed" texture (Fig. 10M) Erosive, sharp or rarely progressive basal boundary	3D megaripple migration of fluvial deposits (Miall, 1978) and aeolian erosion surface attributed to aeolian deflation lag (Clemmensen & Abrahamsen, 1983; Langford & Chan, 1988)
Shd Horizontal laminated sandstones with deflation surfaces	Very fine- to fine-grained sand and medium-grained, well-sorted, rounded quartz grains Beds thickness: 5 cm to 1 m	Horizontal laminations of fine sand alternating with horizontal surfaces of "millet seed" texture (Fig. 10M) Sharp basal boundary	Sheet-flood and aeolian erosion attributed to aeolian deflation lag (Clemmensen & Abrahamsen, 1983; Langford & Chan, 1988)

Sr Ripple cross-laminated sandstones (Fig. 10J)	Very fine- to medium-grained sand with very rarely scattered gravel of quartz Beds thickness: 10 cm to 3.5 m	Asymmetric ripple cross-lamination Ungraded or normally-graded Sharp or erosive basal boundary	Current ripple, lower part of the lower flow regime (Miall, 1978)
Sm Massive sandstones (Figs. 10D, G,12G)	Very fine- to medium-grained sand with occasionally mud-clast and rarely scattered carbonate clasts and gravels (up to 1 cm), occasionally carbonated cement Beds thickness: 10 cm to 3m	Massive occasionally including mud-clasts (Fig. 10F) and more rarely carbonate clasts Erosive or sharp basal boundary,	Subaerial hyperconcentrated density flow or subaqueous high-density turbidity current (Lowe, 1982; Mulder & Alexander, 2001); rapid suspension fallout (Postma, 1990)
SF Sandy heterolithic	Heterolithic sandy facies composed of very fine- to fine-grained sands interbedded with 0.5 mm to 40 cm thick beds of silts Beds thickness: 10 cm to 2.5m	Massive or very finely laminated Erosive or sharp basal boundary	Subaerial hyperconcentrated density flow (Lowe, 1982; Mulder & Alexander, 2001) or rapid suspension fallout (Postma, 1990) alternating with fine deposition from suspension

SFl Laminated sandy heterolithic	Heterolithic sandy facies composed of very fine- to medium-grained sand interbedded with 0.5 to 50 cm thick beds of silts Beds thickness: 10 cm to 9 m	Indeterminate bioturbation, more rarely *Diplocraterion* or *Planolites*	Massive or very finely laminated sands and silts interbedded with asymmetric current ripples and horizontal laminations and/or oscillatory symmetric ripples Sharp and erosive basal boundary Occasionally fluid escape features and mud cracks	Current and wave ripples, tractive current or subaerial high-density flow alternating with deposition from suspension in a shallow water environment
Stb Bioturbated trough cross-bedded sandstones	Fine- to coarse-grained sand, with mud-clasts and rarely carbonate clasts (cm to 10 cm) Beds thickness: 10 cm to 5 m	Indeterminate bioturbation, *Diplocraterion* (Fig. 11B) and *Planolites*	Trough cross stratifications (h=10 cm to 2 m, λ=m to dam) (Fig. 11A) Sharp or erosive basal boundary occasionally underlying by mud-clast Ungraded or normally-graded Occasionally fluid escape features and contorted bedding (Fig. 11C)	3D megaripple migration reworked by biological activity in a subaqueous environment
Shb Bioturbated horizontal	Very fine- to medium-grained sand Beds thickness:	Indeterminate bioturbation	Horizontal and sub-horizontal laminations Ungraded or	Sheet-flood reworked by biological activity at a relative shallow depth or at the top of mouth bar (Pollard et al., 1982; Marshall,

laminated sandstones	10 cm to 5.5 m		normally-graded Erosive, sharp or progressive basal boundary	2000; Hinds et al., 2004)
Sb Bioturbated massive sandstones (Fig. 11D)	Very fine- to medium-grained sand with very rarely scattered carbonate clasts and gravels Beds thickness: 10cm to 4 m	Indeterminate bioturbation, *Thalassinoides*, *Diplocraterion*, very rarely *Planolites (Supplementary Data Fig. 1A, E)*	Erosive, sharp or rarely progressive basal boundary	Reworking of sand deposits by biological activity in a marine environment
Msig Marine tidal deposits	Fine-grained sand with reactivation surfaces of medium-grained sand and very fine-to coarse-grained sandy limestones (Fig. 11E) Beds thickness: 50 cm to 6 m	Indeterminate bioturbation, *Scolicia* like	Sigmoidal trough cross stratifications (h=10 cm to 40 cm) draped by thin siltstones (pluri-mm to pluri-cm, Fig. 11F), rare tidal bundles and hearing bones features (Fig. 11G) Ungraded or rarely inversely graded Erosive or sharp basal boundary occasionally overlain by mud-clasts and coarse quartz grains Occasionally fluid escape feature, contorted bedding	Tidal bars (Olariu et al., 2012; Dalrymple, 2010)

Srw Ripple and oscillatory cross-laminated sandstones (Fig. 11H)	Very fine- to fine-grained sand Beds thickness: 5 cm to 1 m	Indeterminate bioturbation	Asymmetric ripple cross-laminated and oscillatory cross-laminated sandstones Erosive, sharp or progressive basal boundary Rarely fluid escape features	Current and wave ripple in a shallow water environment
SFb Bioturbated sandy-heterolithic (Fig. 11I, 12E)	Same lithology as SF Beds thickness: 10 cm to 4.5 m	Indeterminate bioturbation, *Diplocraterion (Supplementary Data Fig. 1A)*	Massive Ungraded or normally graded Sharp or erosive basal boundary	Subaqueous high-density turbidity current (Lowe, 1982; Mulder & Alexander, 2001) or rapid suspension fallout (Postma, 1990) alternating with deposition from suspension reworked by biological activity
Sbf Bioturbated massive bioclastic sandstones	Coarse-grained bioclastic sandstones with occasionally carbonated cement Beds thickness: 10 to 1.5 m	Indeterminate bioturbation Usually abundant indeterminate bioclasts, crinoid fragments, bivalves, brachiopods, gastropods and echinoid spines (Fig.	Massive Erosive, sharp or occasionally progressive basal boundary	Marine bioclastic sandflat reworked by biological activity in a marine environment

		11K, L, M)		
Stf Bioclastic trough cross-bedded sandstones	Fine- to coarse-grained carbonated sand to sandy-limestones Beds thickness: 20 cm to 1.5m	Indeterminate bioturbation Abundant crinoids fragments, gastropods, brachiopods, bivalves, echinoid spines	Trough cross stratifications (h=10 cm to 80 cm, λ=m) Ungraded or normally-graded Erosive or sharp basal boundary	3D megaripple migration reworked by biological activity in a marine environment, marine sandflat (Dalrymple, 2010)
ST Trough cross-bedded sandstones	Fine- to medium-grained sand usually rich in micaceous elements with silts at the base of the foresets Beds thickness: 80 cm to 15.5 m	Indeterminate bioturbation, rarely *Palaeophycus*, *Planolites* (Sup. Data 1B, C) and very rarely Crustacea burrows	Trough cross stratifications (h=20 cm to 3.5 m, λ=several m to dam, Angles of dip: 11° to 29°) occasionally underlined by medium sand (Fig. 12A, H) Tangentially based foresets either draped by silts frequently bioturbated (2 cm to 30 cm thick) or by counter-current asymmetric ripples (Fig. 12B, C, D) Erosive or sharp basal boundary Ungraded or rarely normally graded Fluid escape features, contorted bedding (Fig.	3D marine dunes migration

			12A) and more rarely small syn-sedimentary faults (10 cm to 20 cm)	
Srb Bioturbated ripple cross-laminated sandstones (Fig. 12F)	Very fine- to medium-grained sand with occasionally mud-clasts at the base Beds thickness: 10 cm to 1.5m	Indeterminate bioturbation	Asymmetric ripple cross-laminations Sharp basal boundary but occasionally erosive basal boundary overlain by mud-clasts	Current ripple reworked by biological activity in subaqueous environment
Silts				
F Siltstones	Silts and silty-clays Beds thickness: 5 cm to 1.70 m		Massive (Fig. 10H) Occasional mud cracks (Fig. 10I)	Deposition from suspension, temporary water body (Miall, 1996)
Fl Laminated fine heterolithic	Heterolithic facies composed of silts and silty-clays interbedded with 1 cm to 10 cm thick beds of very fine-grained sandstones Beds thickness: 5 cm to 1.5 m		Very fine laminated silts interbedded with asymmetric current and oscillatory ripples, horizontally laminated or massive sand (Fig. 10G) Occasional dessication cracks	Deposition from suspension alternating with waning flow or overbank, temporary water body (Miall, 1996)

Fb Bioturbated siltstones (Fig. 12G)	Silts and silty-clays Beds thickness: 5 cm to 2 m	Indeterminate bioturbation, *Diplocraterions*, *Thalassinoides, Planolites* Indeterminate bivalves and brachiopods	Massive Occasional mud cracks	Deposition from suspension reworked by biological activity in a permanent water body
Flb Bioturbated laminated fine heterolithic (Fig. 12E)	Same lithology as Fl Beds thickness: 5 cm to 3 m	Indeterminate bioturbation, *Thalassinoides, Planolites*, rarely *Psilonichnus, Scolicia* "like" Indeterminate bivalves and brachiopods	Same sedimentary structures as Fl	Deposition from suspension alternating with waning flow reworked by biological activity within a permanent water body
Limestones				
Cf Bioclastic limestone (Fig. 11J)	Sandy limestones or limestones usually intensively bioclastic, very rarely with scattered gravel of quartz Beds thickness: 5 cm to 1 m	Indeterminate Crinoids fragments, bivalves, brachiopods, gastropods, very rarely ammonoids, echinoid spines Indeterminate bioturbation on the top of beds	Massive Erosive or sharp basal boundary	Sandflat or storm deposits (Dalrymple, 2010)

1569

1570

	Sedimentary architecture	Depositional environment and Paleocurrents
,	Compound cosets and more rarely isolated dunes sets of 20 cm to 34.5 m thick (AT, Fig. 9A, F). Root traces: PR, rarely PRmo in the upper portion of dunes (Supplementary Data Fig. 2D1, EC3). Ichnotaxa: *Taenidium*, occasionally marine bioturbation (*Planolites* or D*iplocraterion,* Fig. 9J, Supplementary Data Fig. 3A1, C1)	Migration of aeolian dunes. Overlain by paleosols indicated by vertical root traces. Occasionally overlain by marine flooding episodes indicated by marine burrowing organism at the top of dunes. 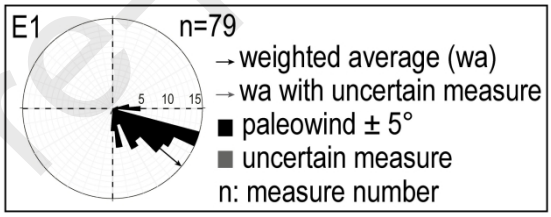
	Aeolian planar deposits of pluri-cm to 3.5 m (Ar, Ah).	Dry aeolian sand-sheets or interdunes (Hunter, 1977; Clemmensen & Abrahamsen, 1983).
	Aeolian planar deposits with adhesion structures of pluri-cm to 2.6 m thick (Aa, Ar). Root traces: PR very rarely at the top of beds.	Alternation of dry and wet aeolian sand-sheets or wet aeolian sand-sheets and interdunes (Hunter, 1977; Kocurek & Nielson, 1986).
Sh,	Isolated or stacked channelled sandstones deposits of dm- to 6 m-thick composed of vertical association Gm, Gt, St, Sh, Sm, Sr). This association, either complete or truncated,	Braided river (e.g. Miall, 1996), paleocurrent oriented towards the south-west

is interbedded with some silt facies (F, SF)..	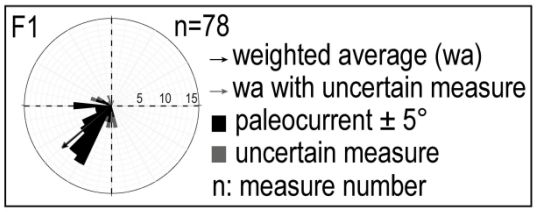
Tabular beds of isolated or stacked fining upward sandstones bodies of planar bed of density flows and occasionally tractive currents of decimetric to 4.5 m thick (Gm, Sm, Sh, St, Sr) interbedded with silts and heterolithic facies of pluri-cm to pluri-dm- thick (SF, SFl, F, Fl). Root traces and pedogenetic carbonates nodules observed at the top of sandstones beds (PR, Pr, Pn).	Unchanneled streamflows (i.e. sheet-flood).
Silt and heterolithic facies of decametric to 9 m thick (F, Fl) interbedded with some sandstone beds pluri-cm to 2.5 m thick (Sm, Sh, Sr, SF, SFl). Ichnotaxa: *Taenidium*. Mudcracks usually observed. Thin root traces with or without carbonates concretion often observed at the top of silty levels (respectively Pr and Prn, Supplementary Data Fig. 2B1, B3). Nodular carbonate Pn (Supplementary Data Fig. 2A), frequently observed few decimentres below Prn. Rarely PR.	Waning flood and overbanks within a distal alluvial plain in semi-arid conditions (carbonate nodules: Hasiotis & Bourke, 2006; Hasiotis *et al.*, 2007).
Planar beds of streamflow deposits pluri-dm to 2.2 m thick usually with deflation surfaces (Shd, Std, Sh, Sr) interbedded with aeolian deposits	Ephemeral unchanneled streamflows deposits within an arid alluvial plain (Clemmensen & Abrahamsen, 1983;

pluri-dm thick (Ar).	Langford & Chan, 1989).
Compound cosets or isolated sandstone and conglomerate bars, displaying soft sediment deformation (often contorted bedding and more rarely water escape features), characterized by: - channelled sequences (pluri-cm to 5 m-thick Gm/Gt, St, Stb, Sb) - tabular beds (pluri-cm- to 1.5 m Stb/St, Shb/SF/SFb, Fb/F). alternating with pluri-cm to pluri-dm silty deposits (Fb, F). Ichnotaxa: *Diplocraterion* and *Planolites*. Microfossils: foraminifers. Root traces (PR) at the top of the megaripples (Supplementary Data Fig. 2C2).	Distributary mouth bars (Postma, 1990, Bhattacharya, 2010) and unconfined flow (i.e. sheet-flood, tabular beds). Large dispersion of the paleocurrents, mainly towards the SW, occasionally to the SE, resulting of longshore currents. 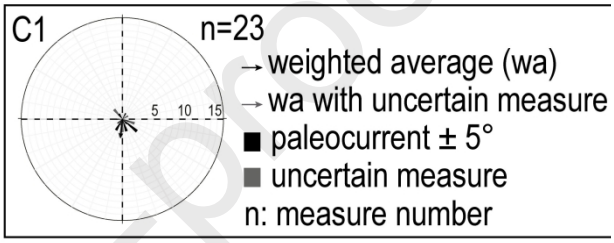
Compound cosets of tidal sand bars (Msig) of 60 cm to 5.5 m thick with some erosional basal boundary. Marine bioclastic sands pluri-cm to 2 m thick (Gm, Stf, Sbf, Stb, Sm, Sh, Sb) and sandy limestones (Cf, 10 cm to 1. 5m) interbedded with marine silty facies and rarely heterolithic facies (Flb, Fb, SFb) of 10 cm to 1.5m thick. Ichnotaxa: *Thalassinoides*, *Scolicia* like, rarely *Psilonichnus* and maybe *Bichordites* like (Supplementary Data Fig. 3D, E, F). Macrofossils: brachiopods (Productids, Spiriferida and undetermined), gastropods (*Anomphalus* sp.,	Supra- to intertidal environment with storm wash-over deposits.

	Bellerophon, Turilicone, planispiral shells) bilvalves (*Wilkingi*a sp. and undetermined), nautiloids (*Tainoceras* and undetermined), crinoids, massive and fenestrate bryozoans, echinoid spines (Fig. 11K to M). Occasionally mud-cracks and rarely fluid escape features. <u>Root traces</u> at the top of sandy limestones (PR, rarely Pr).	
ial -	Alternation of bioturbated sandstones and siltstones with current-ripples and horizontal laminations of pluri-cm to 5.5 m (Sh, Sb, Sm, Shb, Srw, Sr, Srb, Stb, SFl, SFb) with silty facies (Flb, Fl, F, Fb). The sedimentary structures are current-ripples and horizontal bedding and very rarely oscillatory ripples. Mud-cracks. <u>Root traces</u> at the top of sandstone (PR) and siltstones (Pr, Pn, Prn) or d<u>esiccations cracks</u>	Coastal plain or marsh with paleosols development.
p,	Isolated large-scale dunes or compound cosets (40 cm to 15.5 m thick) frequently intensively bioturbated (ST) grading laterally into bioturbated sandstones (Sb, Shb, Sr, Srb), siltstones (Flb, Fb, Fl, F) and heterolithic facies (SF) (Fig. 12H). Usually contorted bedding can be observed. <u>Ichnotaxa</u>: Undifferentiated or maybe *Planolites*, *Palaeophycus* and maybe very rarely Crustacean burrows. <u>Microfossils</u>: foraminifers.	Offshore bar or detached shoreface deposits (Plint, 2010), with a longshore current oriented to the SSE, periods of subaerial exposure attesting by vertical root traces. 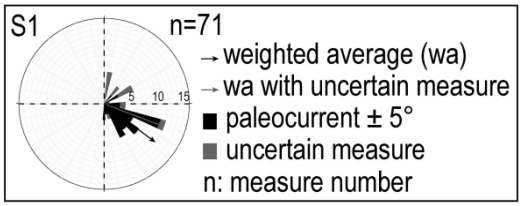

	Root traces: PR or PRmo at the top of compound cosets (Supplementary Data Fig. 2D2, D3).	
), F -	Often bioturbated heterolithic facies (10 cm to 4.5 m thick, SFb, SFl) alternating with pluri-cm to metric silty facies usually bioturbated (Flb, Fb, Fl, F) and sandstone beds often bioturbated (pluri-cm to 3 m thick, Sm, Sb, Shb, Sr, Srb, Srw) (Fig. 12H, I). The most representative sedimentary structures are current-ripples, oscillatory-ripples and some horizontal bedding. Ichnotaxa: *Diplocraterion* and *Planolites*, occasionally "*Scolicia*" like and maybe rarely *Palaeophycus.* Root traces: occasionally PR the top of sandstones deposits and Pr in silty-clay deposits (Supplementary Data Fig. 2B2)	Subtidal environment with periods of subaerial exposure.

1571

1572